NISTIR 6447

The Reactions of Zinc Vapor with ZIRCALOY-4 and Pure Zirconium

Maureen Williams

NIST

The Reactions of Zinc Vapor with Zircaloy-4 and Pure Zirconium

Maureen Williams

ABSTRACT

Title of Thesis: The Reactions of Zinc Vapor with Zircaloy-4 and Pure Zirconium

Degree candidate: Maureen Elizabeth Williams

Degree and year: Master of Science, 1999

Thesis directed by: Dr. Manfred Wuttig
                    Department of Materials and Nuclear Engineering
                    and Dr. William J. Boettinger
                    National Institute of Standards and Technology

The need for the Nuclear Regulatory Commission to extend the existing licenses on temporary dry storage containers of spent radioactive fuel, coated with zinc paint to prevent corrosion, from 20 years to 100 years initiated this study. The investigation of the reaction of zinc vapor on unirradiated samples of Zircaloy-4 and nuclear grade zirconium at various temperatures between 650 °C and 800 °C is presented.

Through various analytical techniques: optical metallography, scanning electron microscopy (SEM), transmission electron microscopy (TEM), and X-ray diffraction, the reaction of zinc vapor with Zircaloy-4 and nuclear grade zirconium was investigated. The temperatures for the diffusion experiments were based on the Zn-Zr binary phase diagram. Temperatures below 750 °C were chosen to remain in the hexagonal close-packed (hcp) α zirconium phase, yet high enough to insure that a reaction would occur in a reasonably short period of time. Extrapolation to 350 °C would then be used to estimate the effect during dry storage. However, experiments at 725 °C indicated the presence of β zirconium, so additional experiments with nuclear grade zirconium at temperatures above 725 °C were performed to confirm the eutectoid reaction temperature in the binary phase diagram and to investigate the solubility of zinc in zirconium.

DISCLAIMER

Commercial equipment and materials are identified in order to adequately specify certain procedures. In no case does such identification imply recommendation or endorsement by the National Institute of Standards and Technology, nor does it imply that the materials or equipment identified are necessarily the best available for the purpose.

Acknowledgements

TABLE OF CONTENTS

LIST OF TABLES

LIST OF FIGURES

1   INTRODUCTION

Spent nuclear fuel storage in the United States is a major concern for both the power utilities that operate nuclear power plants and the government regulating authority, the Nuclear Regulatory Commission (NRC). The NRC needs to extend the existing licenses on temporary dry storage containers from 20 years to 100 years, because of the delay in the completion of the Yucca Mountain permanent storage facility in Nevada. The Department of Energy (DOE) is currently doing a viability assessment study of the Yucca Mountain repository. According to the department estimates, if the facility is licensed in 2002, the site could begin to receive radioactive material by 2010 [1].

When a spent fuel bundle containing as many as 300 individual fuel rods is removed from a reactor core, it is placed in a pool of water for approximately five years to radioactively "cool". The "cooled" fuel bundle is then loaded underwater (to limit radioactive exposure) into a steel storage container called a cask. The loading of the spent fuel may take up to a week. When the loading is completed the cask is removed from the water, vacuum dried, and the top sealed by welding. The internal temperature of the dry cask storage system (DCSS) is expected to equilibrate at approximately 350 °C during normal dry storage. However, the maximum internal temperature may reach 570 °C during vacuum drying [2]. The DCSS containing this spent fuel then remains on site at the power plant. This is the current method of temporary storage until the high-level radioactive waste site at Yucca Mountain is ready [3].

During the underwater spent fuel loading, corrosion of the steel cask produced radioactive iron particles that contaminated the storage pool filters. In recent years, the practice of coating the inside of the DCSS with zinc paint was implemented to prevent this corrosion. However, the introduction of zinc in the sealed storage system may possibly cause problems with the fuel rod material Zircaloy-4 (a zirconium alloy containing 1.5 wt. % tin, 0.2 wt. % iron, and 0.1 wt. % chromium) [4]. The Zircaloy-4 tubes that contain the fuel are referred to as fuel cladding. If the reaction layer between the Zircaloy-4 and zinc vapor given off by the paint at 350 °C is large enough to degrade the fuel cladding and cause cracks or gross ruptures during the dry storage, then the transfer of the spent fuel in the casks to the permanent repository may be in jeopardy. For example, if the cladding failed and spent uranium oxide (UO_2) fuel piled up in the bottom of the container, then fuel retrieval would become a major problem and a water leak in such a case could possibly cause the fuel to become critical causing a nuclear reaction of thermal neutrons [5].

This study does not take into consideration the effects of radiation or the approximately 100 μm zirconium oxide layer that forms on the fuel cladding while it is in the reactor core. All of the samples are unirradiated and have not been preoxidized. Parallel experiments using both Zircaloy-4 and nuclear grade zirconium exposed to zinc vapor from α-brass (Cu-30 wt. % Zn) were conducted below 800 °C. The temperatures for the diffusion experiments were based on the Zn-Zr binary phase diagram. Temperatures below 750 °C were chosen to remain in the α hcp zirconium phase, yet high enough to insure that a reaction would occur in an experimentally accessible time

frame. Extrapolation of these high temperature results to 350 °C would then be used to estimate the effect during dry storage. However, experiments at 725 °C indicated the presence of β zirconium, so additional experiments with nuclear grade zirconium at temperatures above 725 °C were performed to confirm the eutectoid reaction temperature in the binary phase diagram and to investigate the solubility of zinc in zirconium. The main questions to be addressed in this study are : a) will the zinc vapor react with the Zircaloy-4 alloy and pure nuclear grade zirconium, b) how deep will the reaction go, and c) what phases are in the reaction. This thesis will show that a reaction does occur, the depth of penetration is measured and the phases formed are identified.

2   BACKGROUND

The Zn-Zr phase diagram , shown in Figure 1 [6], is an important starting point to understanding the possible zinc reactions with nuclear grade zirconium as well as the zirconium alloy Zircaloy-4. However, the Zn-Zr binary system is not well defined in the Zr-rich side as indicated by the dashed lines on phase diagram. Experiments performed on nuclear grade zirconium exposed to zinc vapor will clear up some of the uncertainty in this region of the phase diagram, specifically the eutectoid temperature and the solubility of Zn in α-Zr.

2.1   Zinc - Zirconium Phase Diagram
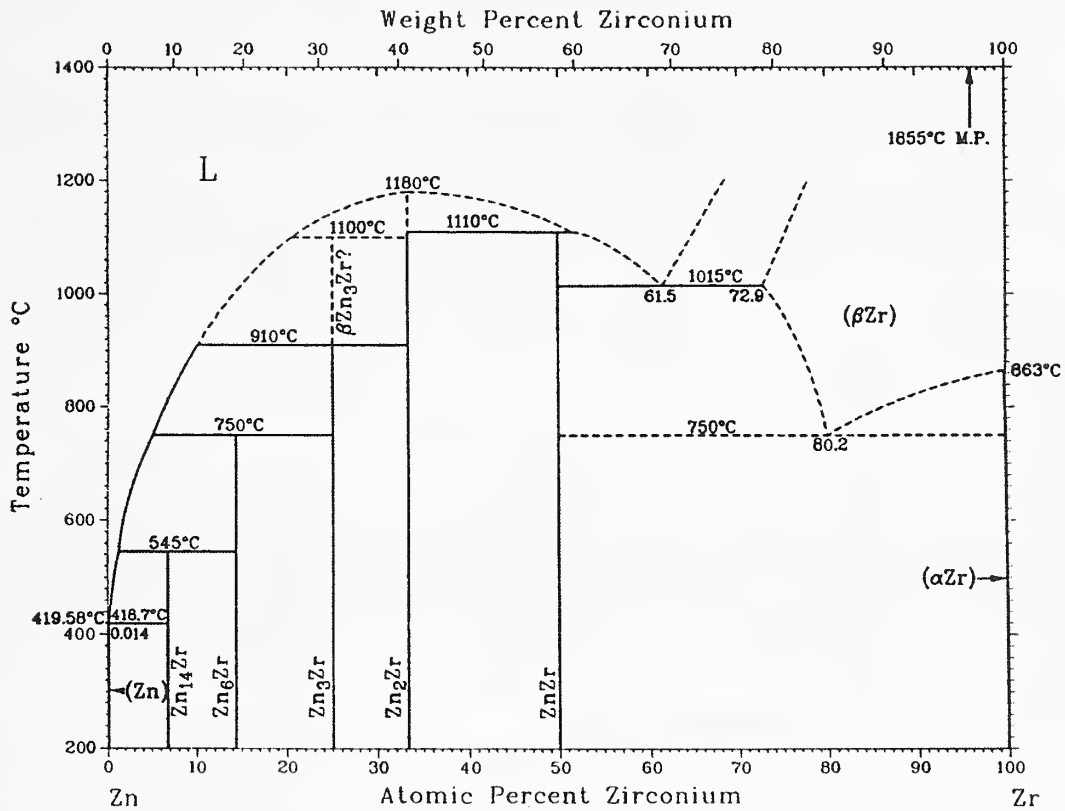
Figure 1. Zn-Zr phase diagram (from *Binary Alloy Phase Diagrams*, Vol.3, 3542, 1990 ASM International, Materials Park, Ohio)

2.2 Intermetallics and Crystallography

In the Zn-Zr phase diagram there are eight intermetallics [6,7] reported and listed in Table 1. Note that three of the intermetallics, $Zn_{22}Zr$, Zn_2Zr_3, and $ZnZr_2$ are not shown in the currently assessed Zn-Zr phase diagram in Figure 1. The lattice parameters, space groups and atomic structure prototypes are also listed in Table 1.

Table 1 Composition, Lattice Parameters, Space Group and Prototype of Phases in the Zn-Zr Binary Phase Diagram from the Literature

Phase	Composition at. % Zr	Lattice parameter (Å)	Space group	Prototype
(Zn)	0	$a = 2.664$ $c = 4.946$	$P6_3/mmc$	Mg
$Zn_{22}Zr$ (e)	?	$a = 14.103$	$Fd\overline{3}m$	…
$Zn_{14}Zr$	6.67	…	$Fd\overline{3}m$	…
Zn_6Zr	14.3	…	…	…
Zn_3Zr	25	$a = 8.16$ $c = 16.23$	…	…
Zn_2Zr	33.3	$a = 7.394$	$Fd\overline{3}m$	Cu_2Mg
ZnZr	50	$a = 3.336$	$Pm\overline{3}m$	CsCl
Zn_2Zr_3 (e)	60.5	$a = 7.633$ $c = 6.965$	$P4_2nm$	Al_2Gd_3
$ZnZr_2$ (e)	66.7	$a = 3.303$ $c = 11.26$	$I4/mmm$	$MoSi_2$
(βZr)	72.9 to 100	$a = 3.546$	$P6_3/mmc$	Mg
(αZr)	100	$a = 3.232$ $c = 5.147$	$Im\overline{3}m$	W

Note: (e) Not shown in the phase diagram.

2.3 Invariant points

Table 2 [6] lists the invariant points for the Zn-Zr system. The two reactions of greatest interest in this study are the allotropic transformation and the eutectoid reaction. Elemental zirconium under goes an allotropic phase transformation at 863 °C from a high temperature β body-centered cubic (bcc) structure to a low temperature α hexagonal close-packed (hcp) structure. At the eutectoid temperature of 750 °C, on the zirconium rich side of the phase diagram, high temperature β transforms into α-Zr and the intermetallic ZnZr ($\beta \rightarrow \alpha$-Zr + ZnZr). However, one author suggests [8] that an additional metastable intermetallic phase $ZnZr_2$ can sometimes form producing two two phase fields of α-Zr + $ZnZr_2$ and $ZnZr_2$+ZnZr. In this case the eutectoid reaction would be $\beta \rightarrow \alpha$-Zr + $ZnZr_2$.

Table 2 Invariant Points of Zn-Zr Binary Phase Diagram

Reaction	composition at% Zr			Temperature °C	Reaction Type
$L \leftrightarrow Zn$........	0			419.58	Melting
$L \leftrightarrow (Zn) + Zn_{14}Zr$....	0.014	0.01	6.67	418.7	Eutectic
$L + Zn_6Zr \leftrightarrow Zn_{14}Zr$..	1.1	14.3	6.67	545	Peritectic
$L + Zn_3Zr \leftrightarrow Zn_6Zr$...	4.4	25.0	14.3	750	Peritectic
$L + Zn_2Zr \leftrightarrow Zn_3Zr$...	10.0	33.3	25.0	910	Peritectic
$L \leftrightarrow Zn_2Zr$...............	33.3			1180	Congruent
$L + Zn_2Zr \leftrightarrow ZnZr$....	51.8	33.3	50	1110	Peritectic
$L \leftrightarrow Zn_3Zr + (\beta{-}Zr)$	61.5	50	73	1015	Eutectic
$(\beta{-}Zr) \leftrightarrow ZnZr + (\alpha Zr)$	80.2	50	100	750	Eutectoid
$L \leftrightarrow \beta{-}Zr$...............	100			1855	Melting
$\beta{-}Zr \leftrightarrow \alpha{-}Zr$............	100			863	Allotropic

2.4 Solubility

There are no data reported on the solubility of Zn in Zr [6]. However, in this study, composition profiles of nuclear grade zirconium exposed to zinc vapor revealed a small solubility of approximately 2 at. % zinc. These findings will be discussed in Section 6.5.

2.5 Material Properties of Zirconium and Zircaloy-4

Two properties of zirconium that make it useful for nuclear applications are low thermal-neutron capture cross section (i.e. transparency to thermal neutrons) and high corrosion resistance [9]. The Zircaloy-4 cladding provides the structural support for the uranium oxide (UO_2) fuel and the alloy's transparency to thermal neutrons allows the neutrons produced by fission of this fuel to pass through the cladding. Zirconium is a highly reactive metal and a stable protective oxide layer naturally forms resulting in a corrosion resistant surface [10]. The corrosion resistance of the Zircaloy-4 cladding protects the fuel in the reactor environment from the high temperature water and steam, typically 350 °C in a pressure water reactor [11].

3 THEORY OF DIFFUSION REACTIONS

Sub-sections one through six will provide a summary of diffusion theory in the following order: 1) mechanisms of atomic movement, 2) the number of phases that can form in a two component system based on the Gibbs phase rule, 3) thermodynamics to explain local equilibrium at different times in the non-equilibrium diffusion process, 4) the rate of diffusion, 5) multicomponent effect on diffusion and 6) growth mechanism.

3.1   Diffusion Mechanisms

Diffusion is defined as the movement of atoms in a material [12]. The two main types of atomic movement in a solid solution are interstitial and vacancy. Interstitial diffusion occurs when atoms move into the spaces of the atomic lattice not normally occupied. Vacancy diffusion occurs when atoms substitute on vacant lattice sites. In this study the main type of atomic movement is by vacancy diffusion. As the temperature of a material increases, the number of vacancies increases as well as the jump frequency allowing more opportunity for atomic movement. The atomic movement through the crystal can occur either in the bulk lattice structure or along the grain boundaries.

3.2   Diffusion in Binary Systems

The number of phases that are present in an equilibrium system can be found based on degrees of freedom. The Gibbs phase rule states that a system in equilibrium with C number of components and P number of phases will have F number degrees of freedom, as expressed in equation 1.

$$F = C - P + 2 \qquad (1)$$

The degrees of freedom are the number of intensive variables, such as temperature, pressure, and chemical potential that can be independently varied without necessarily changing the phase present in the equilibrium system [13]. Therefore the degrees of freedom must be zero in order to completely describe the system [12]. With the pressure fixed equation 1, becomes equation 2

$$F = C - P + 1 \qquad (2)$$

and in binary two component system with C=2, reduces to equation 3.

$$F = 3 - P \qquad (3)$$

Thus, the degrees of freedom for a single phase field is two, requiring both temperature and composition to be specified to completely describe the system. In a two phase field of the phase diagram, only one degree of freedom remains. Either the composition of the phases or the temperature must be specified to completely describe the system. So, once the temperature is fixed, then the composition of the two phases are fixed and vice versa if the compositions of the phases are fixed then the temperature is fixed. This means in a binary isothermal diffusion couple a two phase reaction zone, i.e. "containing precipitates or wavy interfaces" [14] can not exist. However, in multicomponent systems (three components or more) a two phase region can exist in the diffusion couple since the degrees of freedom would be greater than one and allow for composition variation of the phases at a fixed temperature.

3.3   Phase Equilibrium

Knowing the activity of a surrounding vapor, allows the local equilibrium at the surface to be estimated.
The equilibrium between the metal surface and the vapor [15] occurs when the chemical potential, μ, of each component is equal in the two phases, as expressed in equation 4

$$\mu_A^\alpha = \mu_A^\beta, \ \ \mu_B^\alpha = \mu_B^\beta \quad . \qquad (4)$$

Often the activity, a, is defined by equation 5

$$\mu = \mu^o + RT \ln a \qquad (5)$$

where μ^o is the chemical potential at a reference state, R is the gas constant equal to 8.314 J/mole Kelvin, and T is the temperature in degrees Kelvin. So from equation 5 when the two phases are in equilibrium the activities are also equal, as expressed in equation 6

$$a_A^\alpha = a_A^\beta, \ \ a_B^\alpha = a_B^\beta \quad . \qquad (6)$$

The common tangent to the Gibbs free energy curves G^α and G^β gives the phase compositions, where the two phases have equal chemical potentials. This is shown schematically in Figure 2 where the free energy is plotted as a function of composition and the chemical potentials are at the endpoints of the tangent line.
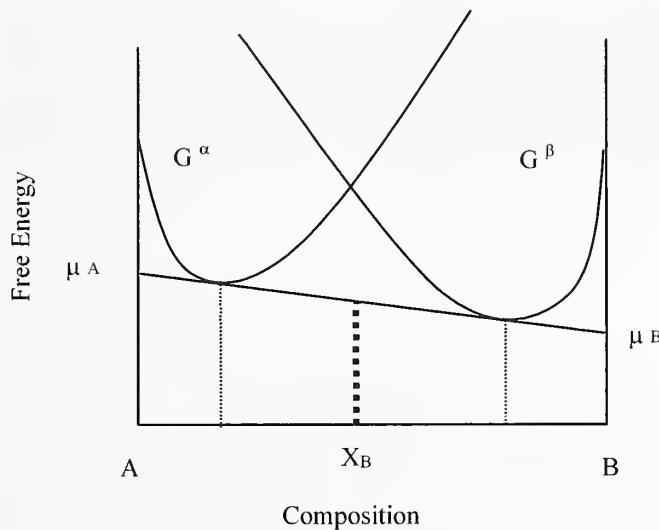
Figure 2. Schematic of free energy as a function of composition at constant pressure and temperature. X_B represents the alloy composition.

In this study, the activity of the zinc leaving the α-brass is equal to the activity of the zinc arriving at the surface of the zirconium and the local equilibrium can be defined. This situation is illustrated in Figure 3.
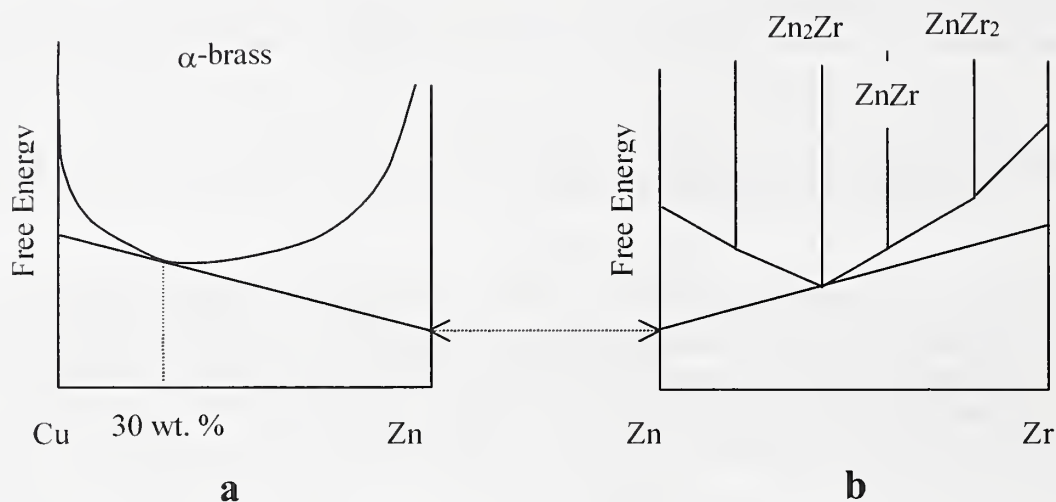
Figure 3. Schematic of equal chemical potentials a) from the surface of the α-brass and b) of the single phase layer that forms on the surface of the zirconium. In this case Zn$_2$Zr would be the surface phase formed on the Zr surface.

A thermodynamic assessment of zinc in α-brass (Cu-30 wt. % Zn) [16] was used to find the activity and chemical potential of zinc at the surface of the bulk zirconium or Zircaloy-4 at the seven different heat treatment temperatures and the results are listed in Table 3 (the reference state for these calculations was based on the melting point of zinc, 419.5 °C). See Section 4.2.1, equation 12, for a discussion of the vapor pressure of pure zinc.

Table 3 Activity and Chemical Potential of Zinc in α-Brass (Cu-30 wt. % Zn)

Temperature (°C)	Activity of Zinc in α-Brass	Chemical Potential of Zinc in α-Brass (Joules/mole)	Vapor Pressure of Pure Zinc (kPa)	Partial Pressure of Zinc in α-Brass (kPa)
650	5.1404×10^{-2}	-2.2781×10^{4}	3.59	0.185
670	5.5459×10^{-2}	-2.2679×10^{4}	4.98	0.276
700	6.1786×10^{-2}	-2.2527×10^{4}	7.85	0.485
712	6.4396×10^{-2}	-2.2466×10^{4}	9.44	0.608
725	6.7272×10^{-2}	-2.2399×10^{4}	11.4	0.767
775	7.8786×10^{-2}	-2.2145×10^{4}	22.48	1.771
800	8.4792×10^{-2}	-2.2017×10^{4}	30.83	2.614

3.4   Rate of Diffusion

Diffusion is the movement of atoms and this movement can be described by measuring the flux, J, through a cross sectional unit area of material, the units for flux are mass/cm^2 s. Fick's first law, equation 7 equates the flux, with the product of the diffusion coefficient, D, and the concentration gradient where c is concentration and x is the distance,

$$J = -D \frac{\partial c}{\partial x} \quad . \quad (7)$$

The diffusion coefficient is defined in equation 8 as

$$D = D_0 \exp(-Q/RT) \quad , \quad (8)$$

where D_0 is the diffusion constant (cm^2/s) for a specific material, Q is the activation energy (J/mole), R is the gas constant = 8.314 J/mole Kelvin and T is the temperature in degrees Kelvin.

To express the change in concentration as a function of time and assuming the diffusion coefficient does not change with concentration then Fick's second law can be expressed as equation 9,

$$\frac{\partial c}{\partial t} = \frac{\partial}{\partial x} \left[D \frac{\partial c}{\partial x} \right] = D \frac{\partial^2 c}{\partial x^2} \quad . \quad (9)$$

Assuming the sample length of the bulk material is infinite compared to the length of the diffusion region, then Fick's second law can be solved by using the error function, $erf(z)$. Where $erf(z)$ is defined by equation 10

$$erf(z) = \frac{2}{\sqrt{\pi}} \int_0^z e^{-z^2} dz \ . \qquad (10)$$

The error function is available in any computer spread sheet. Assuming an infinite source of zinc vapor at the surface of nuclear grade zirconium, which is initially free of any solute, the surface concentration will remain constant over time. For the boundary conditions $x = 0, t \geq 0, c = c'$ and at $x = \infty, t \geq 0, c = 0$. The concentration of the zinc diffusing into the bulk zirconium is given by equation 11, where c' is the fixed surface concentration,

$$c(x,t) = c'\left[1 - erf\left(\frac{x}{2\sqrt{Dt}}\right)\right] \ . \qquad (11)$$

Figure 4 illustrates two concentration profiles increasing with time, both have fixed surface concentrations: a) profile of a single phase solid solution and b) profile of a solid solution with an intermetallic phase at the surface.
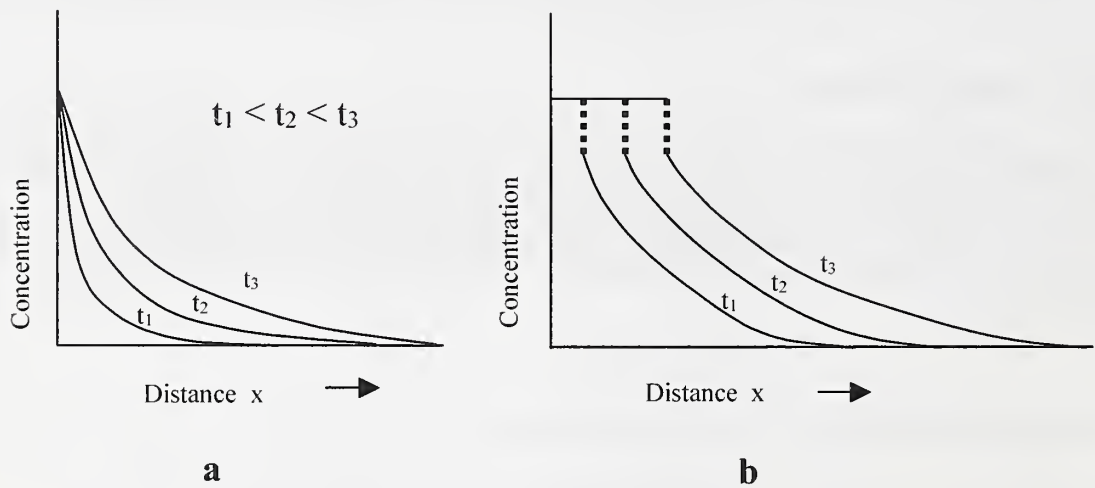
Figure 4. Typical concentration profiles for fixed surface concentration increasing with time. a) single phase in a solid solution b) solid solution containing a surface intermetallic phase.

The reaction of zinc vapor with the Zircaloy-4 and nuclear grade zirconium produced intermetallic layers growing parallel to the surface. As illustrated in Figure 5, the presence of plateaus on the composition profile indicates a stoichiometric intermetallic

compound, and a line that slightly slopes indicates a phase with some range of homogeneity. The vertical jump in concentration indicate an interphase interface.
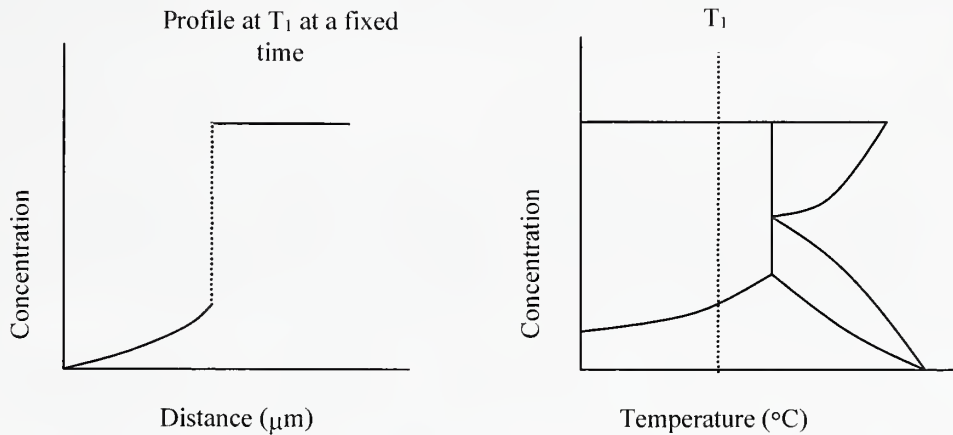
Figure 5. A schematic of a composition profile at T_1 and how it relates to a binary phase diagram.

3.5   Diffusion in Multicomponent / Multiphase Systems

In the Zircaloy-4 samples the alloying elements, Sn, Fe, and Cr can change phase boundaries, cause additional phases to form, and produce two phase regions. Experimental problems associated with multiphase regions will be discussed in Section 4.3.3.

3.6   Growth mechanisms – Parabolic

To determine of the type of growth, the depth of the reaction zone is measured at different times at the same temperature. Based on the depth of the reaction zone, x, the time exponent, n, can be determined by plotting the experimental data as $x = (Kt)^n$. If n equals one, the growth is linear , if n equals 1/2 the growth is parabolic and will form a straight line when the data is plotted in the form $\dfrac{x}{\sqrt{t}} = \sqrt{K}$ where $\sqrt{K}$ is the slope of the line. The value of the growth constant K is then found by squaring the slope. The growth constant should follow the expression for a diffusion process as

$K = K_0 \exp\left(\dfrac{-Q}{RT}\right)$. Where K_0 is the growth constant coefficient in cm^2/s , Q is the

activation energy in J/mole, R is the gas constant equal to 8.314 J/mole Kelvin and T is the temperature in Kelvins. In general, the growth constant K is a function of the diffusion constants, D, of all the layers and the concentration at all the interfaces from the phase diagram.

11

4   EXPERIMENTAL

4.1   Materials

4.1.1   Sample Materials

Diffusion experiments were performed on three types of non-radioactive samples: nuclear grade zirconium, Zircaloy-4 tube reduced extrusion (TREX), and Zircaloy-4 tubing. Nuclear grade zirconium is produced by refining commercial grade zirconium which contains approximately 1.5 to 4.5 wt. % hafnium [12]. Since hafnium is a neutron absorbing element (hafnium's thermal neutron capture cross section is 133×10^{-24} cm^2 compared to Zircaloy-4 with 0.22×10^{-24} cm^2 [12]), it is not desirable for nuclear fuel cladding and is removed by a liquid chemical process [13]. The nuclear grade zirconium for this study was cut from ingot # 340667-Zr provided by Oremet-Wah Chang*, and it contains 58 parts per million by weight (ppm) of hafnium (ASTM limit for hafnium in nuclear grade material is 100 ppm [4]). Table 4 lists the range of trace element composition in this ingot.

Table 4 Trace Element Composition of Nuclear Grade Zirconium Ingot # 340667-Zr as given by Oremet-Wah Chang, an Allegheny Teledyne Company*

Element	ppm	Element	ppm
Al	20	Na	5
B	0.025→0.25	Nb	50
C	34	Ni	35
Ca	10	O	60→300
Cd	0.25	P	4→5
Cl	5	Pb	4→5
Co	10	Si	25
Cr	50	Sn	10
Cu	10	Ta	50
Fe	50→90	Ti	25
H	3	U	1
Hf	**57→58**	V	25
Mg	10	W	25
Mn	25		
Mo	10		
N	12→19		

Values are in parts per million by weight (ppm)

Zircaloy-4 is a dilute α zirconium alloy containing 1.5 wt. % tin, 0.2 wt. % iron, and 0.1 wt. % chromium. This alloy is used as nuclear fuel cladding in pressure water reactors. The exact dimensions of the fuel cladding vary according to the reactor design but typical dimensions are 4 m in length, 11 mm in outside diameter with a wall thickness of 0.75 mm [17]. Both the TREX and tubing (lot # 3ME13-8) were provided by McDermott Technology, Inc* (formerly Babcock & Wilcox R&D) in Lynchburg, Virginia.

The Zircaloy-4 TREX has a 6.35 cm outside diameter and a wall thickness of 1.27 cm and is the first step in tube production [18]. The Zircaloy-4 tubing as-received was already stress relieved through annealing at 500 °C by the supplier. This tubing has dimensions of 11 mm outside diameter and a wall thickness of 0.75 mm. It is the final step in cladding production before the tube surface is pre-oxidized and ready to receive fuel.

4.1.2 Zinc Vapor Source

The zinc vapor source used for this study was α-brass (Cu-30 wt. % Zn) that contains less than 0.01 wt. % Fe. A 1.27 cm diameter rod was cleaned with ethyl alcohol and the rod was turned on a lathe to remove the surface layer. After the surface layer was removed, addition machining was done to produce thin brass filings. The brass filings were then cleaned in an ultrasonic bath with acetone and then ethyl alcohol and stored in a desiccator.

4.2 Procedures

4.2.1 Sample Preparation

The Zircaloy-4 TREX and the nuclear grade zirconium samples were sliced from bulk material with a diamond saw. All samples were cut to approximately the same dimensions, 12 mm long, 3 mm wide and 1.5 mm thick. The surfaces were ground, finishing with wet 600 grit SiC paper, and then polished with a 6 μm diamond suspension. The samples were then cleaned with acetone and ethanol and air-dried. Samples were encapsulated in a quartz tube under a vacuum of 1.33×10^{-5} Pa. The samples were annealed at approximately 700 °C for six d in order to relieve any stresses introduced by the extrusion process and sample preparation. After air cooling the tube containing the annealed samples was broken and each sample was polished to 1/4 μm finish, cleaned and then individually encapsulated with high purity α-brass filings under a vacuum of 1.33×10^{-5} Pa. A single Zircaloy-4 tubing sample (pre-annealed at 500 °C) and was cut into a 25 mm length, cleaned and encapsulated with brass. At the highest experimental temperature of 800 °C, the zinc vapor pressure over brass is 30.83 kPa as given in Table 3. The vapor pressure of copper at 800 °C is insignificant. This was calculated using equation 12, where P is in mm Hg and the temperature T is in Kelvins [19].

$$\log_{10} P = \frac{-0.05223(a)}{T} + b \qquad (12)$$

For liquid zinc in the temperature range between 600 °C and 985 °C the values of the constants are a=118,000 and b=8.108. The constant values for copper (a=468,000 and b=12.344) are only valid in the temperature range between 2100 °C and 2310 °C so during the heat treatments the brass filings are only a source of zinc vapor. Table 3 in section 3.3 lists the zinc vapor pressure at other heat treatment temperatures.

4.2.2 Heat Treatment

A 5 cm inside diameter vertical Marshall tube furnace was used for the heat treatments. A Nichrome cylindrical container, 8.25 cm tall with a 3.75 cm inside diameter, with lid was placed in the middle of the furnace hot zone and allowed to equilibrate at the furnace temperature. This produced an isothermal hot zone within the container. The furnace tube above and below the container was packed with firebrick to prevent convection currents in the tube. The encapsulated sample was then placed inside the Nichrome container. The sample was monitored by a type K (chromel-alumel) sheathed thermocouple placed through the lid to within 5 mm of the sample. This thermocouple was connected to a large external aluminum isothermal plate that serves as the cold junction reference. This external panel was then connected to a temperature data acquisition board in a computer. The furnace temperature was maintained with a separate type K thermocouple connected to a temperature controller.

4.2.3 Temperature Calibration

The furnace was calibrated using a pure element encapsulated in quartz. The furnace temperature is set approximately 10 °C below the element's melting point. Once the furnace is equilibrated, the encapsulated standard is placed in the Nichrome container. The furnace temperature is raised by one degree and the standard is removed and visually inspected for melting and then placed back in the Nichrome container and the furnace is then allowed to re-equilibrate. This process is repeated until the standard melts. The temperature of the thermocouple monitoring the standard is recorded and then all other thermocouples are placed in that furnace one at a time and their temperatures are recorded. The thermocouples were Inconel sheathed type K with the thermocouple junction tip grounded to the sheath. Using three different furnaces set at the melting points of lead, zinc, and aluminum (327 °C, 419 °C, and 660 °C respectively), each thermocouple had a three point calibration. All thermocouples were corrected using these results.

4.2.4 Sample Quenching

At the end of the diffusion anneal the samples were quenched in water at room temperature. The sample was immersed in the water and then the quartz tube was

broken using a hammer. The time from removal of the sample from the furnace until the quartz tube is broken underwater was approximately 5 s to 10 s.

4.2.5 Choice of Heat Treatment Temperatures

The experiments were performed with Zircaloy-4 TREX, Zircaloy-4 tubing, and nuclear grade zirconium encapsulated with brass filings in vacuum at 650 °C, 670 °C, 700 °C, 712 °C, 725 °C, 775 °C, and 800 °C. The initial choice of temperatures for the diffusion experiments were based on the Zn-Zr binary phase diagram, shown in Figure 1. Temperatures just below 750 °C were chosen to remain in the hcp α zirconium phase, yet high enough to insure that reaction would occur in the shortest period of time possible. However experiments at 725 °C indicated the presence of β zirconium, so additional experiments with nuclear grade zirconium at temperatures above 725 °C were performed to confirm the eutectoid reaction temperature in the binary phase diagram.

4.3 Characterization

4.3.1 Metallography

All of the samples were cut in cross section and mounted in epoxy resin for optical metallography. The samples were then ground with 400 and 600 grit wet SiC papers and then polished starting with 15 μm diamond suspension and finishing with ¼ μm diamond suspension. The grain size measurement of the Zircaloy-4 tubing, Zircaloy-4 TREX, and nuclear grade zirconium as-received materials was performed using the circular intercept method, ASTM standard test method E112-96 [20], on a ¼ μm diamond polished sample, etched with a solution of hydrofluoric acid, nitric acid and water [21]. The measured grain sizes of the three as received materials, Zircaloy-4 tubing, Zircaloy-4 TREX and nuclear grade zirconium was found to be approximately 2 μm, 10um and 140μm, respectively. After grain size measurements, all of the samples were repolished to a ¼ μm surface finish to remove the chemical etch.

4.3.2 Energy Dispersive Spectrometry

Each sample was examined with a JEOL model 840A* Scanning Electron Microscope (SEM). Using Energy Dispersive Spectrometry (EDS) with elemental standards for zinc, zirconium, tin, iron, and chromium, a compositional line scan was done on each sample. All line scans were preformed with the an accelerating voltage of 20 kV, a probe current of 535 pA, and a 100 s acquisition time. The EDS composition profiles started at the edge of the sample and the electron beam was scanned towards the middle. The SEM electron beam resolution for EDS analysis is ~1 μm and the line scan steps were varied from 0.5 μm to 1.5 μm. The results gave a composition profile and the penetration depth of the zinc diffusion reaction zone.

4.3.3   Complications in the Interpretation of Composition Line Scans

The line scans results of all the samples are shown in Appendix A, Figures A1 through A21. The edge of the sample is always on the left and is highlighted by a white outline produced by the electron beam. The arrow indicates the path of the electron beam. An explanation of interpreting these line scans is in order.

In the profiles of samples exposed to zinc vapor for short diffusion times, the single phase layers were very narrow, on the order of 1 µm or 2 µm thick, so the shelves and steps of the line scans are not well defined because the phase width is approximately the same as the 1 µm resolution of the SEM probe beam. Combined with the beam resolution problem is the number of points measured in this narrow reaction layer zone. Using too many points causes an overlapping and the data appears smeared and taking too few points makes the line scan data appear choppy. So in the short heat treatment profiles the lines representing the separation of two different phase layers is not truly vertical and the plateaus are not truly horizontal. However, the different phases were distinguishable by the change in contrast in the SEM micrographs taken in the compositional backscattered mode. Figure 6 shows an example of a line scan of nuclear grade zirconium exposed to zinc vapor for at 775 °C for 12 d. This scan shows very clearly the plateau of the single phase intermetallic at 50 at. % Zr, the vertical line representing the interface separating the ZnZr intermetallic and the β phase, and the sloping line of the β phase that indicates a range of composition in that phase.
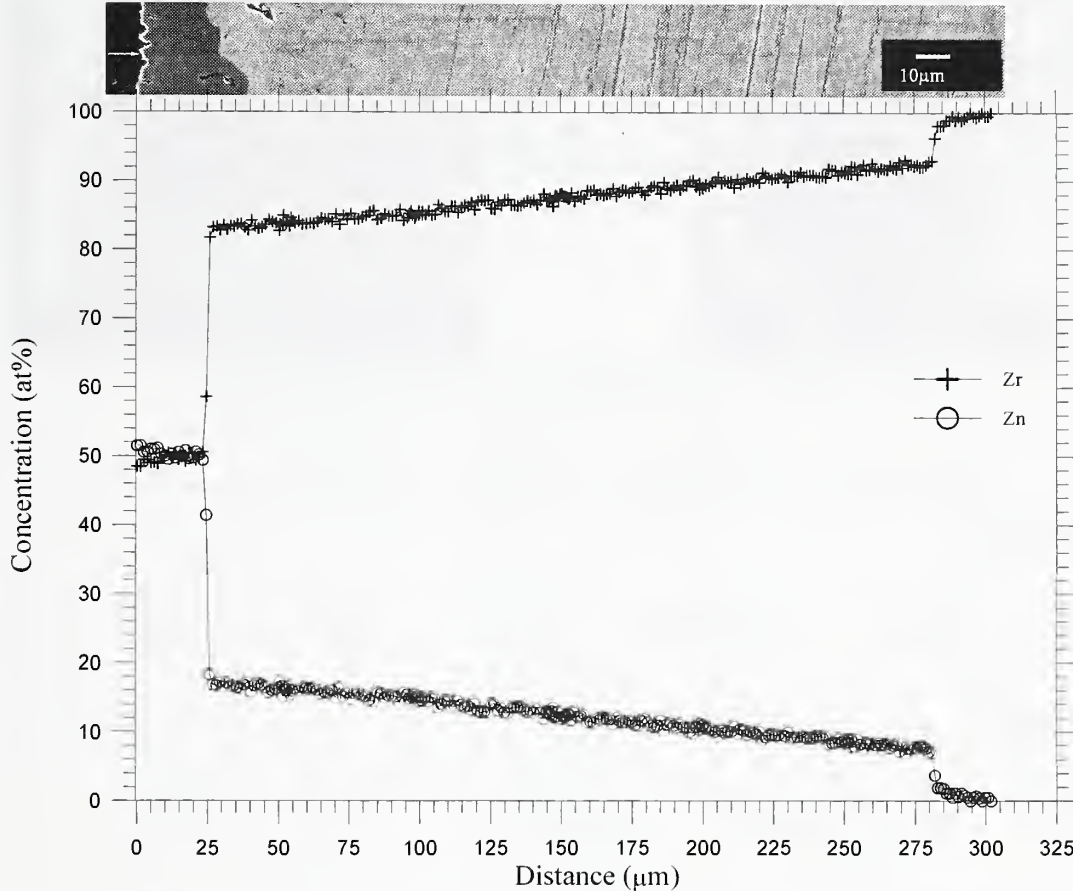
Figure 6. Nuclear grade zirconium exposed to zinc vapor at 775 °C for 12 d. Note the interface between the β phase and α-Zr is not visible.

An example of a line scan with questionable and non-existent plateaus is shown in appendix A Figure A1. This scan of nuclear grade zirconium exposed to zinc vapor at 650 °C for 16 d illustrates the problems of narrow width phases and also too few data points.

For the Zircaloy-4 samples exposed to zinc vapor, two new complications arise due to the multicomponent nature of Zircaloy-4. First, the Fe and Sn atoms appear to substitute on the same lattice sites as the Zn atoms in the intermetallic compounds. So in order to identify the different phases from the line scans only the Zr concentration was typical of the intermetallic stochiometry. The second complication is the formation of a 2 phase layer of light colored precipitates in a dark colored matrix between two layers of single phases. As the line scan crossed this layer, the beam was either overlapping the two phases, measuring an average composition of the precipitates and the matrix, or the beam hit only one the phases and measured the precipitate or the

matrix individually. Therefore the line scans across this 2 phase layer do not give accurate compositions, so individual point measurements were done on each of the phases making up the 2 phase layer separately. The average composition of the individual phases in this two phase region, the matrix and precipitate, were determined by measuring four different points in each phase. The correct compositions of the matrix and precipitates and those results are shown Table 5. The phases were identified as (Zn, Fe, Sn) Zr dark matrix and (Zn, Fe, Sn) Zr_2 as the light precipitate. For simplicity these phases will be abbreviated as (Zn, x)Zr and (Zn, x)Zr_2, respectively, where x represents the Fe and Sn on the Zn sublattice.

Table 5 Composition of Phases in the Two Phase Region

	at% Zr	at% Zn	at% Sn	at% Fe	at% Cr
Light region					
Average	63.78	22.70	2.78	10.41	0.36
Std. Dev.	4.20	4.63	0.51	0.19	0.15
Dark region					
Average	52.78	36.35	0.58	9.55	0.70
Std. Dev.	0.51	0.90	0.18	0.50	0.10

In Figure 7 two line scan profiles of Zircaloy-4 exposed to zinc vapor at 650 °C for 126 d shows: a) the profile when the beam only passes through the matrix phase of the 2 phase layer and b) the profile when the beam passes through the precipitate phase of the 2 phase layer. In order to correctly interpret the line scans both the micrograph and the graph must be carefully evaluated.

18
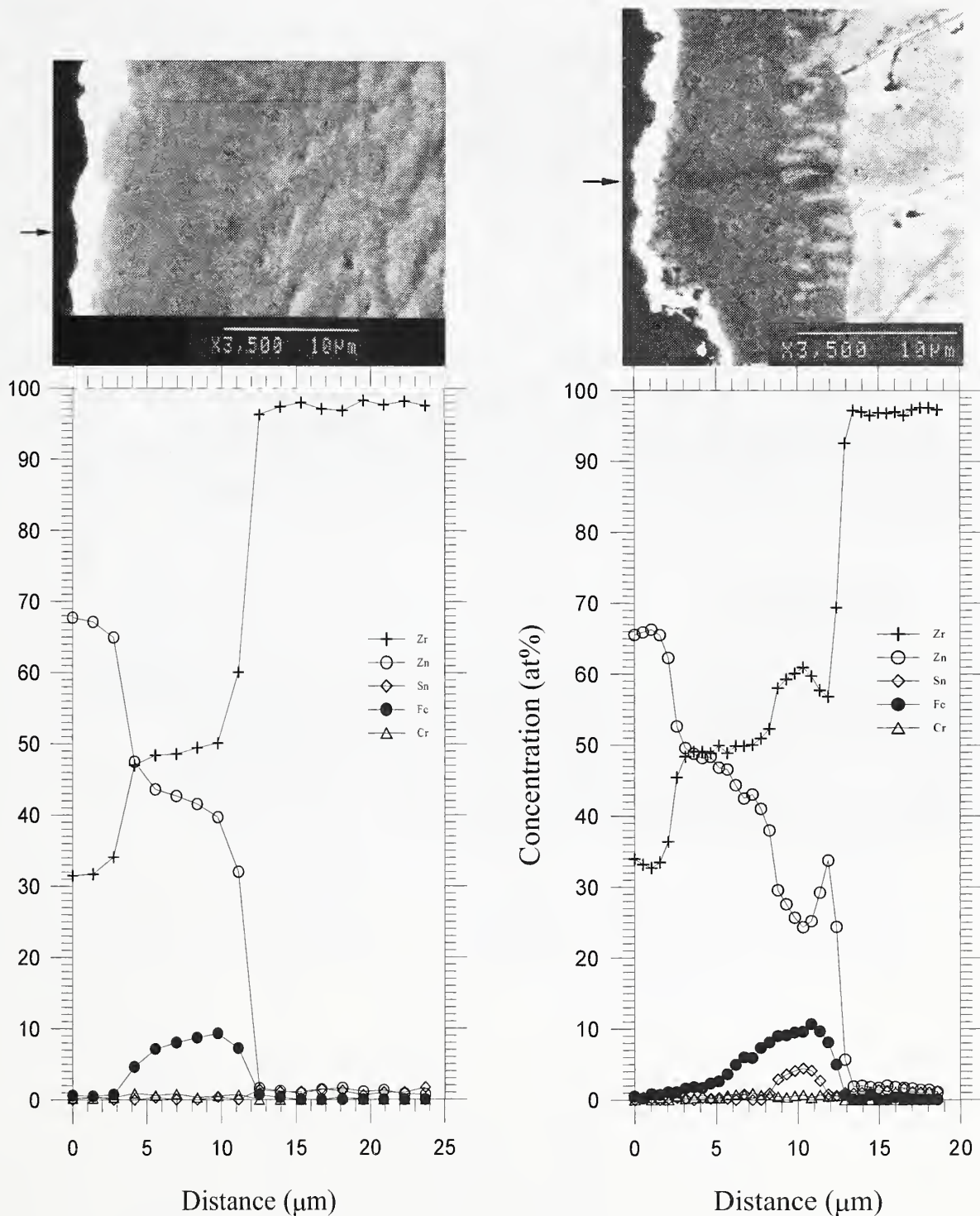
Figure 7. Zircaloy-4 exposed to zinc vapor at 650 °C for 126 d a) the profile when the beam only passes through the matrix phase of the 2 phase layer and b) the profile when the beam passes through the precipitate phase of the 2 phase layer.

4.3.4   X-Ray Diffraction

The X-ray diffraction scans were performed on three samples; Zircaloy-4 TREX, Zircaloy-4 tubing as-received, nuclear grade zirconium as-received, using a theta-two theta Scintag* diffractometer with a copper target at power setting of 45 kV and 40 mA. All scans were done over a two theta range from 20 °to 125 ° at a step size of 0.02 ° and a count time of 10 s per step. The x-ray diffraction patterns of all three samples correspond to the hcp α-Zr phase.

5   RESULTS

In Section 5.1 a brief summary of the phase sequences within the reaction zone will be given. In Section 5.2 the thickness of the individual phases and the overall thickness of the total reaction zone will be summarized. In section 5.3 the details of the microstructure, composition profiles and phase analysis will be discussed. Section 5.4 will follow with an estimate of the growth constant based on the total reaction zone thickness.

5.1   Phase sequences

A two phase layer of $(Zn, x)Zr + (Zn, x)Zr_2$ was only found in the Zircaloy-4 samples. Six distinct phase sequences were observed from the sample surface to the interior in nuclear grade zirconium and Zircaloy-4 exposed to zinc vapor depending on temperature. Table 6 provides a summary the phase sequence of each individual Zircaloy-4 and nuclear grade zirconium sample. To easily distinguish identical phase sequences, each sequence listed in Table 6 is numbered.

20

Table 6 Phase Sequence of Zircaloy-4 and Nuclear Grade Zirconium

Temperature °C	Time (d)	Material	Phase Sequence	
650	16	NGZr w/ brass	1	(Zn_2Zr), $(ZnZr)$, α-Zr
650	64	NGZr w/ brass	1	(Zn_2Zr), $(ZnZr)$, α-Zr
650	16	Zir-4 w/ brass	2	(Zn_2Zr), $(ZnZr)$, 2 phase $(Zn, x)Zr + (Zn, x)Zr_2$, α-Zr
650	64	Zir-4 w/ brass	2	(Zn_2Zr), $(ZnZr)$, 2 phase $(Zn, x)Zr + (Zn, x)Zr_2$, α-Zr
650	126	Zir-4 w/ brass	2	(Zn_2Zr), $(ZnZr)$, 2 phase $(Zn, x)Zr + (Zn, x)Zr_2$, α-Zr
670	21	Zir-4 w/ brass	2	(Zn_2Zr), $(ZnZr)$, 2 phase $(Zn, x)Zr + (Zn, x)Zr_2$, α-Zr
700	4	Zir-4 w/ brass	2	(Zn_2Zr), $(ZnZr)$, 2 phase $(Zn, x)Zr + (Zn, x)Zr_2$, α-Zr
700	10	Zir-4 w/ brass	2b	$(ZnZr)$, 2 phase $(Zn, x)Zr + (Zn, x)Zr_2$, α-Zr
700	32	Zir-4 w/ brass	2	(Zn_2Zr), $(ZnZr)$, 2 phase $(Zn, x)Zr + (Zn, x)Zr_2$, α-Zr
700	12	NGZr w/ brass	1	(Zn_2Zr), $(ZnZr)$, α-Zr
700	32	NGZr w/ brass	1	(Zn_2Zr), $(ZnZr)$, α-Zr
712	11.8	NGZr w/ brass	3	(Zn_2Zr), $(ZnZr)$, $(ZnZr_2)$, α-Zr
725	2	Zir-4 w/ brass	4	(Zn_2Zr) $(ZnZr)$, (β phase), α-Zr
725	11.8	Zir-4 w/ brass	5	$(ZnZr)$, $(ZnZr_2)$, (β phase), α-Zr
725	11.8	Zir-4 w/ brass	6	$(ZnZr)$, 2 phase $(Zn, x)Zr + (Zn, x)Zr_2$, (β phase), α-Zr
725	39	Zir-4 w/ brass	4b	$(ZnZr)$, (β phase), α-Zr

Temperature °C	Time (d)	Material	Phase Sequence	
725	12	NGZr w/ brass	4	(Zn_2Zr), $(ZnZr)$, $(\beta$ phase$)$, α-Zr
725	64	NGZr w/ brass	3	(Zn_2Zr), $(ZnZr)$, $(ZnZr_2)$, $(\beta$ phase$)$, α-Zr
775	12	NGZr w/ brass	4b	$(ZnZr)$, $(\beta$ phase$)$, α-Zr
800	12	NGZr w/ brass	4b	$(ZnZr)$, $(\beta$ phase$)$, α-Zr

Notes:

The "b" means same sequence except for the surface phase, which may have been difficult to detect.

Two morphologies of the 65 to 70 at% Zr phase were observed:
   1. $ZnZr_2$ phase develops as a single phase layer.
   2. Two phase layer of $(Zn, x)Zr + (Zn, x)Zr_2$.

5.2   Individual Intermetallic and Total Reaction Zone Thickness

The region of interest in this study begins with the Zn_2Zr phase at 33 at. % zirconium, the first intermetallic observed on the surface during Zn exposure from brass. Moving in from the surface the next observed intermetallics are the ZnZr, 50 at. % zirconium, and the $ZnZr_2$ containing 67 at. % zirconium. The metastable Zn_3Zr_2 phase containing 60 at. % zirconium was not observed. The phase sequence ends with the α-Zr.

Tables 7 and 8 summarize the thickness of individual phases and the total reaction zone thickness for both the Zircaloy-4 and nuclear grade zirconium samples. The reported uncertainly of the total thickness of the reaction zone measurement is an absolute bounds error. The last column in both Tables is the maximum reaction zone thickness.

Table 7 Zircaloy-4 Phase Thickness and Total Reaction Zone Thickness

Zircaloy-4 Temperature (°C)	Time (d)	Thickness of Zn_2Zr (μm)	Thickness of ZnZr (μm)	Thickness of Two Phase Region (μm)	Thickness of $ZnZr_2$ (μm)	Thickness of Beta Phase (μm)	Total Thickness of Reaction Zone (μm) ± 0.5 μm
650	16	1.0	2.2	1.7 to 2.5	ND	ND	5.7
	64	2.0	2.0	2.8 to 3.7	ND	ND	7.5
	126	2.0	6.2	3.0 to 4.6	ND	ND	12.8
670	21	1.0	2.0	1.4 to 4.0	ND	ND	7.0
700	4	1.0	2.0	1.4 to 2.1	ND	ND	5.1
	10	ND	3.0	2.0 to 3.2	ND	ND	6.2
	32	1.0	3.5	2.8 to 4.0	ND	ND	8.5
725	2	1.5	2.0	≈0.5to 2.0	ND	8.7	12.2
	11.8	1.0	2.0	2.8 to 3.4 [a]	6.0 [a]	15.5	27.5
	39	ND	9.0	ND	ND	40.0	49.0

ND = NOT DETECTED
a = 725 C, 11.8 d - the growth of the 2 phase layer can vary with location on the sample (see Figure 9 in section 5.3.5)

Table 8 Nuclear Grade Zirconium Phase Thickness and Total Reaction Zone Thickness

NGZR Temperature (°C)	Time (d)	Thickness of Zn_2Zr (μm)	Thickness of $ZnZr$ (μm)	Thickness of Two Phase Region (μm)	Thickness of $ZnZr_2$ (μm)	Thickness of Beta Phase (μm)	Total Thickness of Reaction Zone (μm) ± 0.5 μm
650	16	1.5	1.5	ND	ND	ND	3.0
	64	2.0	≈3.0 to 4.0	ND	ND	ND	6.0
700	12		1.0 to 3.2	ND	ND	ND	3.2
	32	2.0	3.0 to 4.2	ND	ND	ND	6.2
712	11.8	1.5	2.5	ND	1.5	ND	5.5
725	11.8	1.0	3.5	ND	4.5	42.0	51.0
	64	≈0.5	6.0 to 8.5	ND	12.0	184.0	205.0
775	12	ND	26.0	ND	ND	261.0	287.0
800	12	ND	40.0	ND	ND	410.0	450.0

ND = NOT DETECTED

5.3   Experimental Line Scan Results

5.3.1   Temperature 650 °C *microstructure/composition profiles /phase analysis*

The microstructure of the Zircaloy-4 sample exposed to zinc vapor at 650 °C for 126 d in Figure 8 shows three planar layers: the ZnZr single phase layer at the edge, the 2 phase layer, and the single phase α-Zr. The edge of the sample on the left has a white outline, this is an edge effect from the electron microscope, and the dashed white line indicates the interface between the ZnZr and the 2 phase layer.
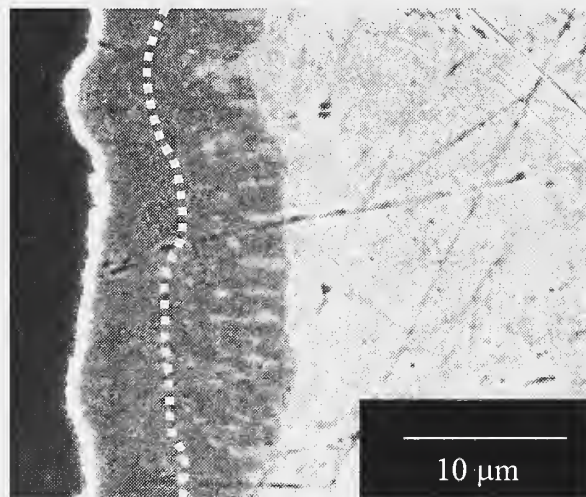
Figure 8. Microstructure of Zircaloy-4 heat treated with zinc vapor at 650 °C for 126 d. The dashed line is the interface between the two visible phases closest to the edge, ZnZr and the 2 phase layer.

However, the line scan profiles of the Zircaloy-4 at 16 d, 64 d and 126 d (Figures A3, A4, and A5) all show that a fourth phase Zn_2Zr (33 at. % zirconium), approximately 1 µm thick at the edge, is also present. The next layer to form is the ZnZr phase (50 at. % zirconium), and then a two phase layer containing a light colored precipitate phase $(Zn, x)Zr_2$ and dark colored matrix phase $(Zn,x)Zr$ previously identified in Table 5. After the two phase region the composition of zirconium varies from approximately 98 to 100 at. % in the bulk α−Zr. In summary the phase sequence for Zircaloy-4 from surface to interior at this temperature is Zn_2Zr, ZnZr, 2 phase $(Zn,x)Zr_2$ + $(Zn,x)Zr$, and α-Zr.

Nuclear grade zirconium was also heat treated at 650 °C for 16 d and 64 d, and as expected, does not contain a 2 phase layer. Both samples have the Zn_2Zr phase at the edge followed by the ZnZr phase. In the 64 d sample the EDS analysis and micrographs indicate the $ZnZr_2$ phase may be present, but with a thickness less than 1 µm. The phase sequence for the nuclear grade zirconium is Zn_2Zr, ZnZr, and α−Zr.

26

5.3.2 Temperature 670 °C *microstructure/composition profiles /phase analysis*

At 670 °C the composition profile of the Zircaloy-4 for 21 d shows that this sample has the same sequence of phases as the 650 °C samples. The Zn_2Zr and $ZnZr$ intermetallic layers and the 2 phase layer all form parallel to the edge.

5.3.3 Temperature 700 °C *microstructure/composition profiles /phase analysis*

At 700 °C the Zircaloy–4 samples at 4 d and 32 d show the same phase sequence as the 650 °C and 670 °C samples. However, the Zn_2Zr phase was not detected on the edge of the 10 d Zircaloy-4 sample.

The nuclear grade zirconium specimen heat treated at 700 °C for 12 d does not contain a 2 phase layer and goes directly from the Zn_2Zr and $ZnZr$ layers at the surface to the α–Zr. However, the line scan of the 32 d sample indicates the $ZnZr_2$ phase may be present, but with a thickness less than 1 μm.

5.3.4 Temperature 712 °C *microstructure/composition profiles /phase analysis*

Nuclear grade zirconium at 712 °C for 11.8 d does not contain a 2 phase layer, but a narrow layer of the $ZnZr_2$ phase is present. It has a different phase sequence then the lower temperature heat treatments. In summary the phase sequence is Zn_2Zr, $ZnZr$, $ZnZr_2$, and α-Zr.

5.3.5 Temperature 725 °C *microstructure/composition profiles /phase analysis*

The results of the 725 °C heat treatments of Zircaloy-4 revealed an unexpected zirconium phase with approximately 85 at. % zirconium in the reported α-Zr + ZnZr region of the Zn-Zr phase diagram below 750 °C. This 85 at. % zirconium phase was later found to be a β phase and will be discussed in Section 6.3.

Three Zircaloy-4 samples were heat treated with brass at 725 °C. Two of the samples were TREX heat treated for 2 d and 11.8 d and the third sample was tubing heat treated for 39 d. In the 2 d sample the phase sequence was Zn_2Zr at the surface followed by $ZnZr$, the 2 phase layer, the β phase and then bulk α-Zr. The 2 phase layer is less than 1 μm wide and is barely visible in micrographs of the two d sample. In the 11.8 d sample the growth of the 2 phase layer varied with location on the sample. In some places the 2 phase layer was absent, in others the precipitate and matrix are both clearly present, and still in other places only a distinct region of the $ZnZr_2$ forms as a non-planar layer between the planar $ZnZr$ and β phase. These three phase sequences are shown in Figure 9, 1) $ZnZr$, β phase,α-Zr 2) $ZnZr$, 2 phase layer, β phase, α-Zr and 3) $ZnZr$, $ZnZr_2$, β phase, α-Zr.
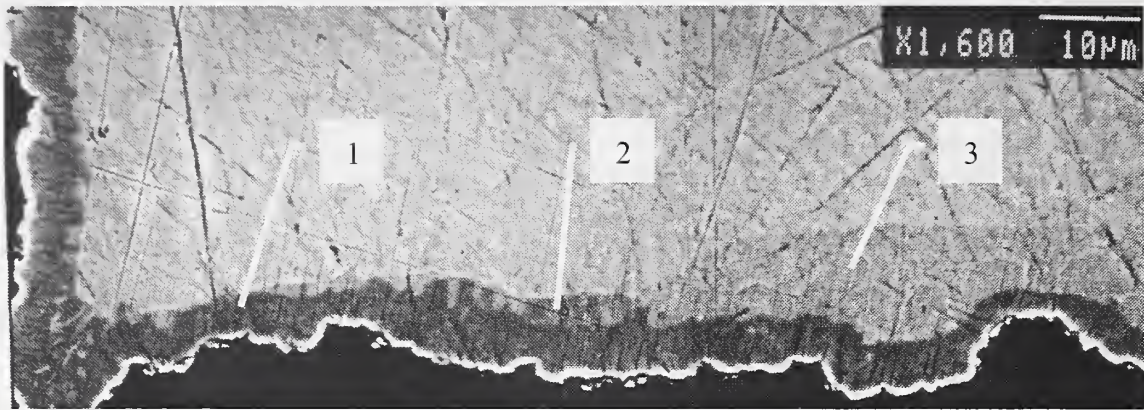
Figure 9. Zircaloy-4 TREX exposed to zinc vapor at 725 °C for 11.8 d. Three phase sequences are shown 1) ZnZr, β phase, α-Zr 2) ZnZr, 2 phase layer, β phase, α-Zr and 3) ZnZr, ZnZr$_2$, β phase, α-Zr.

The 39 d Zircaloy-4 tubing sample does not contain the 2 phase layer or the ZnZr$_2$ and has a phase sequence of ZnZr, β phase, α-Zr.

Nuclear grade zirconium was heat treated at 725 °C for 12 d and 64 d and as expected did not contain the 2 phase layer. Both of these samples had similar phase sequences with Zn$_2$Zr, ZnZr, β phase and α-Zr, but the 64 d also contained the ZnZr$_2$ phase.

5.3.6 Temperature 775 °C *microstructure / composition profiles / phase analysis*

At 775 °C for nuclear grade zirconium, the ZnZr phase forms at the edge but has a non-planar irregular shape. The thickness of this phase varies from approximately 10 μm to 90 μm. In summary the phase sequence is ZnZr, β phase, α-Zr.

5.3.7 Temperature 800 °C *microstructure/composition profiles /phase analysis*

At 800 °C the nuclear grade zirconium has the identical phase sequence as the 775 °C sample. The non-planar growth of the ZnZr phase varied in thickness from 40 μm to 300 μm.

5.4 Estimate of the Growth Constant

The Zircaloy-4 samples were heat treated at 650 °C, 700 °C, and 725 °C at three different times and the nuclear grade zirconium samples were heat treated at 650 °C,

700 °C, and 725 °C at two different times. The depths of the total reaction zone are reported from the surface to bulk α-Zr, see Tables 9 and 10.

Table 9
Reaction Zone Thickness and Growth Constant for
Zircaloy-4

Zircaloy-4			
Temperature (°C)	Time (d)	Total Reaction Zone Thickness (μm) ± 0.5 μm	Estimate of Growth Constant K (cm^2/sec)
650	16	5.7	
	64	8.6	
	126	13.5	1.3305×10^{-13}
700	4	5.2	
	10	6.3	
	32	8.6	3.2291×10^{-13}
725	2	10.0	
	11.8	27.5	
	39	49.0	7.1038×10^{-12}

Table 10
Reaction Zone Thickness and Growth Constant for
Nuclear Grade Zirconium

NGZR			
Temperature (°C)	Time (d)	Total Reaction Zone Thickness (μm) ± 0.5 μm	Estimate of Growth Constant K (cm^2/sec)
650	16	3.0	
	64	6.5	7.4076×10^{-14}
700	12	3.2	
	32	6.3	1.2893×10^{-13}
725	12	51.0	
	64	205.0	6.6484×10^{-13}

The diffusion distance can be expressed by equation 13

$$x = \sqrt{Kt} \qquad . \qquad (13)$$

Where x is the total reaction zone thickness, K is the growth constant of the reaction zone, and t is the diffusion time. This equation can also be expressed as equation 14

$$\frac{x}{\sqrt{t}} = \sqrt{K} \qquad . \qquad (14)$$

As shown in Figure 10, three Zircaloy-4 samples heat treated at 650 °C for 16 d, 64 d and 126 d (with total reaction thicknesses of 5.14 μm, 8.57 μm, and 13.5 μm, respectively) are plotted using equation 14. The linearity of the data point fit represents parabolic growth behavior. The slope of this graph which is the $\sqrt{K}$ was found using the slope intercept method. And the growth constant K is obtained by squaring the value of the slope.
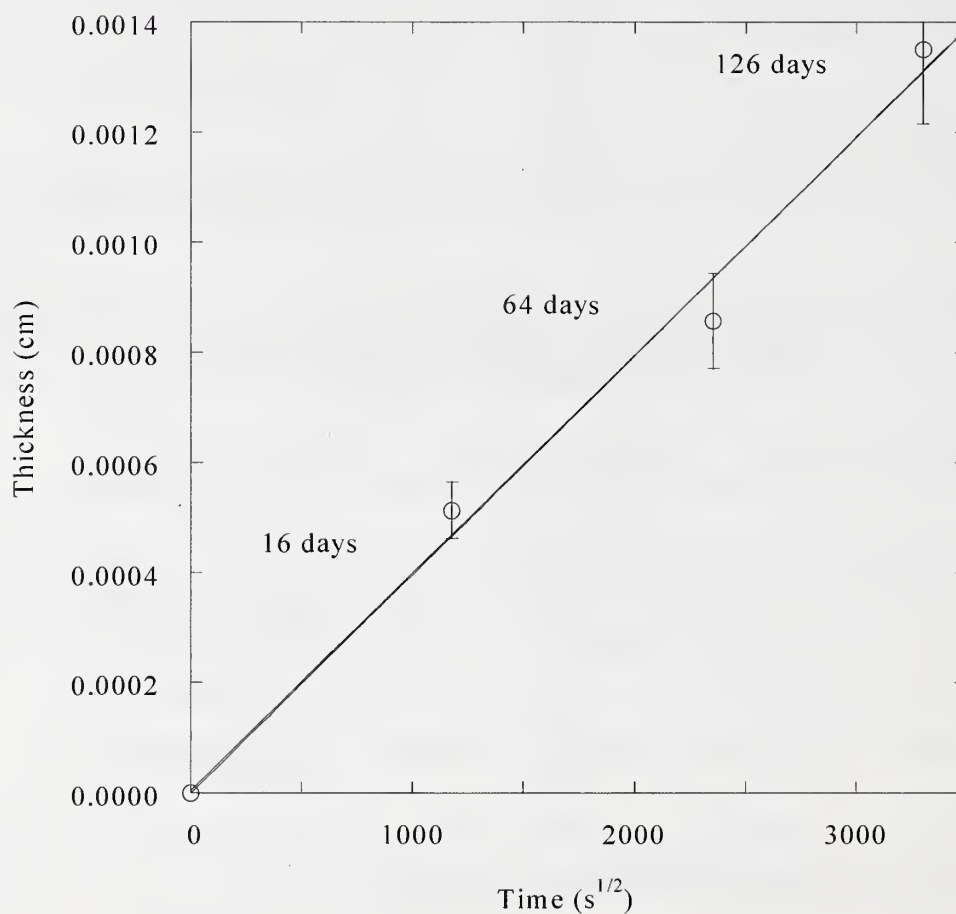
Figure 10. Total reaction zone thickness of Zircaloy-4 heat treated at 650 °C. (The reaction zone thickness measurements have a ± 10 % absolute bounds uncertainty).

The growth constant value, K for all of the Zircaloy-4 and the nuclear grade zirconium samples heat treated at 650 °C, 700 °C, and 725 °C at various times was found using the same method. However, at 670 °C, 712 °C, 775 °C and 800 °C only one sample was heat treated at these temperatures and the parabolic growth constant K was obtained simply by dividing the measured penetration distance squared, divided by the diffusion time.

From the growth constant K found at the various individual temperatures, the activation energy, Q and growth constant coefficient K_0 can then be calculated using the expression in equation 15

$$K = K_0 \exp\left(\frac{-Q}{RT}\right) \quad . \qquad (15)$$

By taking the log of both sides of equation 15 an Arrhenius plot of ln K as a function of inverse temperature in Kelvins, gives an estimate the activation energy Q from the slope and the growth constant coefficient K_0 from the y intercept. The slope of the line is equal to Q/R, where R is the gas constant equal to 8.314 J/mole K. In Figure 11, from the Arrhenius plot of Zircaloy-4 below 725 °C an activation energy Q of 128.56 kJ/mole was calculated and the y intercept gave a growth constant coefficient K_0 equal to 3.741×10^{-6} cm^2/s. The Arrhenius plot of nuclear grade zirconium exposed to zinc vapor at 650 °C, 700 °C and 712 °C, shown in Figure 12, the activation energy 126.65 kJ/mole was measured and the y intercept gave a growth constant coefficient K_0 equal to 1.04×10^{-6} cm^2/s. In Figure 13, the Arrhenius plot of the nuclear grade zirconium at 725 °C, 775 °C and 800 °C containing the β phase gave an activation energy of 554.69 kJ/mole and a growth constant coefficient K_0 equal to $2.03 \times 10^{+14}$ cm^2/s.
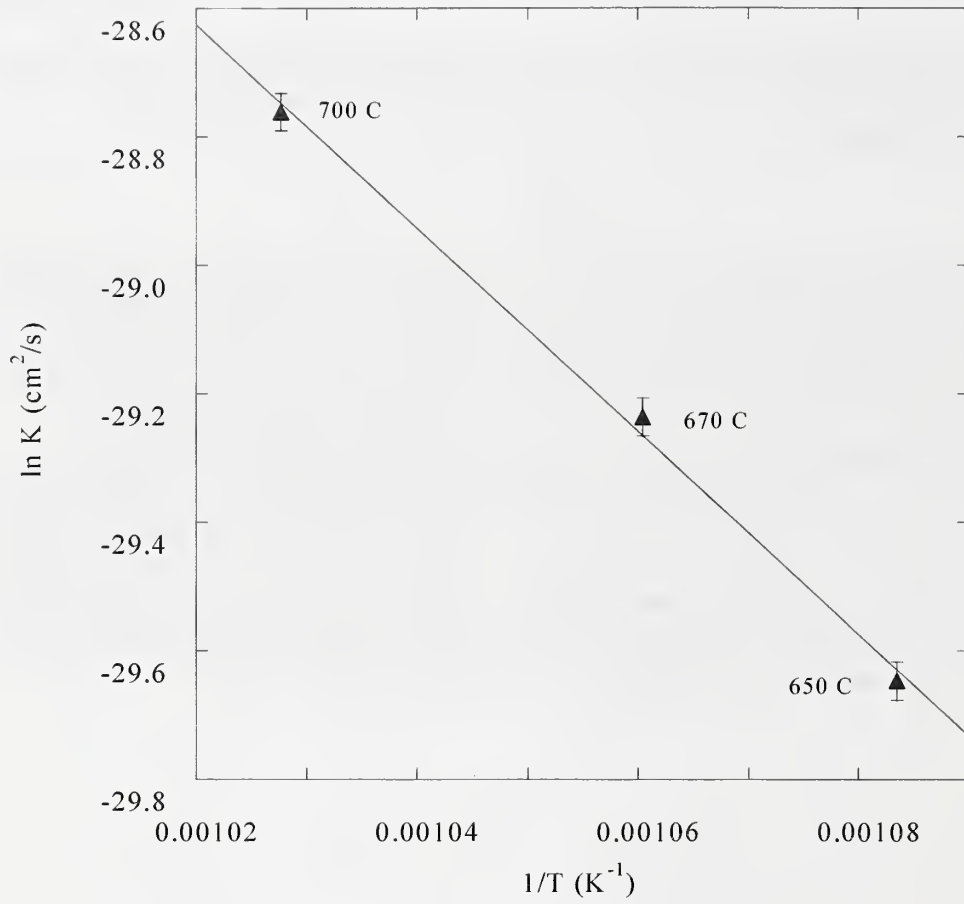
Figure 11. Arrhenius plot of the growth constant K for Zircaloy-4 exposed to zinc vapor at 650 °C, 670 °C and 700 °C. (The data reflects a ± 0.1 % absolute bounds error of ln K value). The measured activation energy is 128.56 kJ/mole.
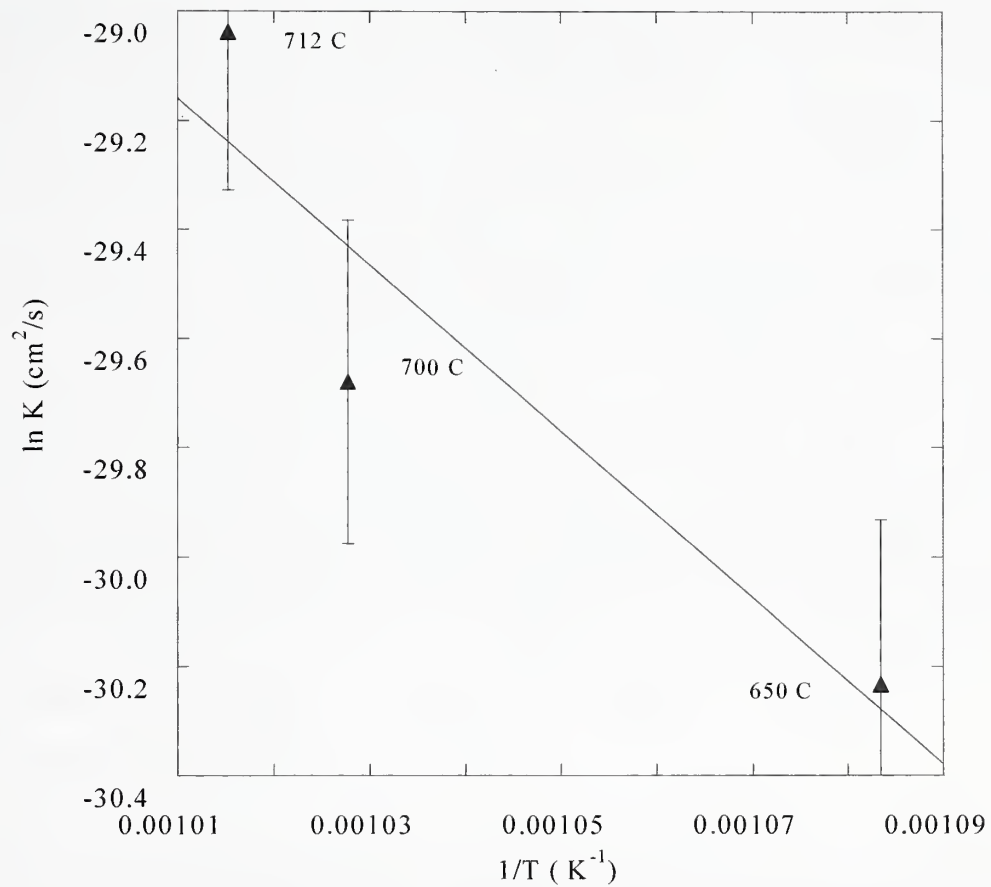
Figure 12. Arrhenius plot of the growth constant K for nuclear grade zirconium exposed to zinc vapor at 650 °C, 700 °C and 712 °C. (The data reflects a ± 1 % absolute bounds error of ln K value). The measured activation energy is 126.65 kJ/mole.
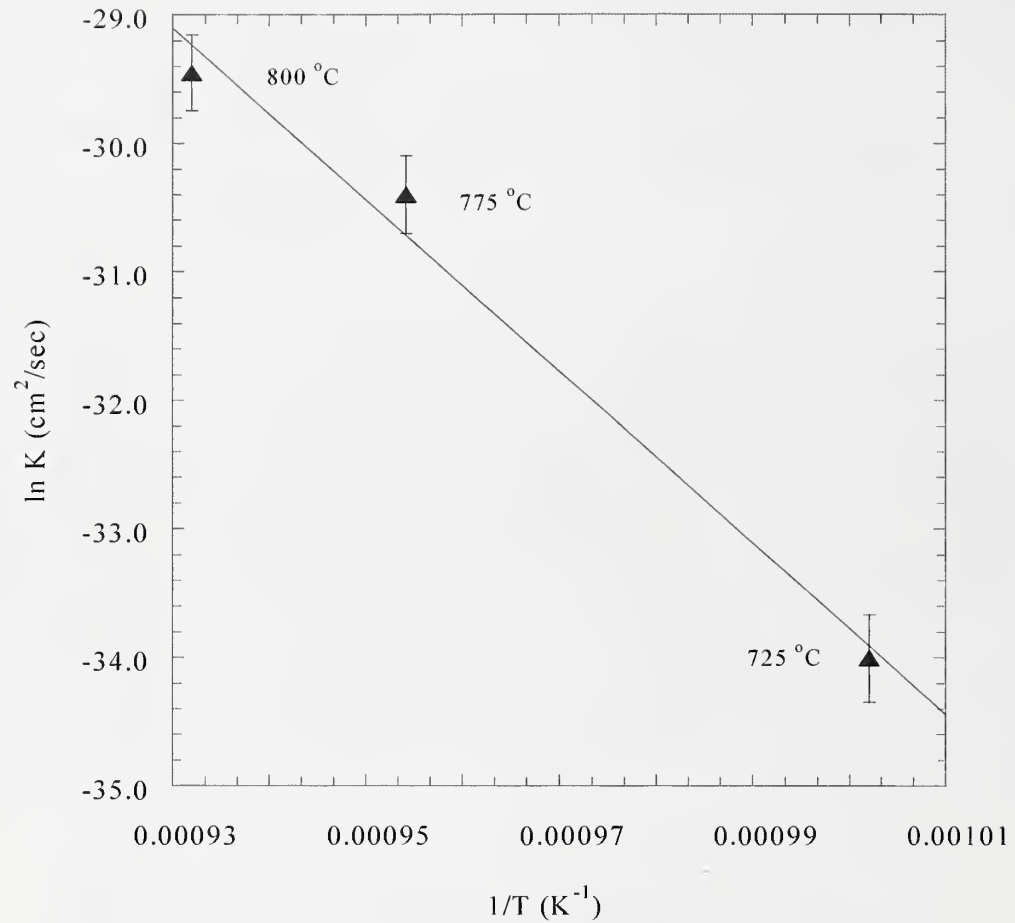
Figure 13. Arrhenius plot of the growth constant K for nuclear grade zirconium exposed to zinc vapor at 725 °C, 775 °C and 800 °C. (The data reflects a ± 1 % absolute bounds error of ln K value). The measured activation energy is 554.69 kJ/mole.

6 DISCUSSION

6.1 Correlation of observed phases to the phase diagram

The observed intermetallic phase growth of the zinc vapor reaction with the Zircaloy-4 and nuclear grade zirconium agrees with the phase sequence of the binary Zn-Zr phase diagram. Zn_2Zr, the 33 at. % Zr phase is the first intermetallic to form on the surface of most of the samples. The ZnZr 50 at% phase is present in all samples. The metastable Zn_2Zr_3, 60 at. % phase was not observed in any of the samples. The $ZnZr_2$, 67 at. % Zr, was only found in the nuclear grade zirconium heat treated at 712 °C for 11.8 d and at 725 °C for 64 d and in the Zircaloy-4 at 725 °C for 12 d. The two phase $(Zn,x)Zr_2$ and $(Zn,x)Zr$ region is only present in the multicomponent Zircaloy-4 samples. The precipitates in this two phase region are Sn and Fe rich surrounded by a ZnZr matrix rich in Fe. The dark matrix $(Zn, x)Zr$ phase composition is approximately 50 at. % Zr, 38.7 at. % Zn, 10 at. % Fe, 0.6 at. % Sn and 0.7 at. % Cr. The precipitate phase is $(Zn, x)Zr_2$ with 64 at. % Zr, 22.6 at. %, 10 at. % Fe, 3.0 at. % Sn and 0.4 at. % Cr. Also the growth of the 2 phase region can vary with location on the sample as shown in figure 9 in section 5.3.5. Three different possibilities exist; 1) the absence of $ZnZr_2$ in any form 2) the two phase region with a light precipitate phase composed of $(Zn,x)Zr_2$ and the dark matrix phase of $(Zn,x)Zr$, or 3) only a distinct region of $ZnZr_2$ is present. In the binary diffusion couple of nuclear grade zirconium exposed to zinc vapor this two phase region does not form in accordance with the Gibbs phase rule, as explained in section 3.2.

6.1.1 Phases below 725 °C

All Zircaloy-4 samples heat treated at 650 °C, 670 °C and 700 °C have the 2 phase $(Zn,x)Zr_2$ + $(Zn,x)Zr$ region, and except for the 10 d 700 °C sample, they all have the Zn_2Zr phase on the surface. All the nuclear grade samples heat treated at 650 °C, 700 °C and 712 °C have the same phase sequence of Zn_2Zr, ZnZr and α-Zr , except the 712 °C sample which also contains the $ZnZr_2$ phase.

6.1.2 Phases Present above 725 °C

At 725 °C and above the β phase is present in all the Zircaloy-4 and nuclear grade zirconium samples. The Zircaloy-4 TREX samples heat treated at 725 °C for 2 d, and 11.8 d contain either the $ZnZr_2$ phase or the 2 phase region, (refer to Figure 9 In section 5.3.5), but these phases are not observed in the Zircaloy-4 tubing sample heat treated for 39 d. In the nuclear grade zirconium samples only the 64 d 725 °C nuclear grade zirconium sample has the $ZnZr_2$ phase. All of the other nuclear grade zirconium samples heat treated at 725 °C, 775 °C, and 800 °C for 12 d do not contain the $ZnZr_2$ phase.

6.2   Growth Rate and Mechanism

The sequence of the reaction layer growth of the nuclear grade zirconium samples at 650 °C, 700 °C, 712 °C, 725 °C, 775 °C, and 800 °C are shown in Figure 14. The black edge along the extreme left side of the micrographs is not part of the sample. The sample edge is just to the right of the black background. The morphology of the surface phases changes from planar layer growth at temperatures 650 °C, 700 °C and 712 °C to non-planar layer growth at temperatures of 725 °C and above. This may be due to the presence of the β phase in the samples at 725 °C, 775 °C and 800 °C.
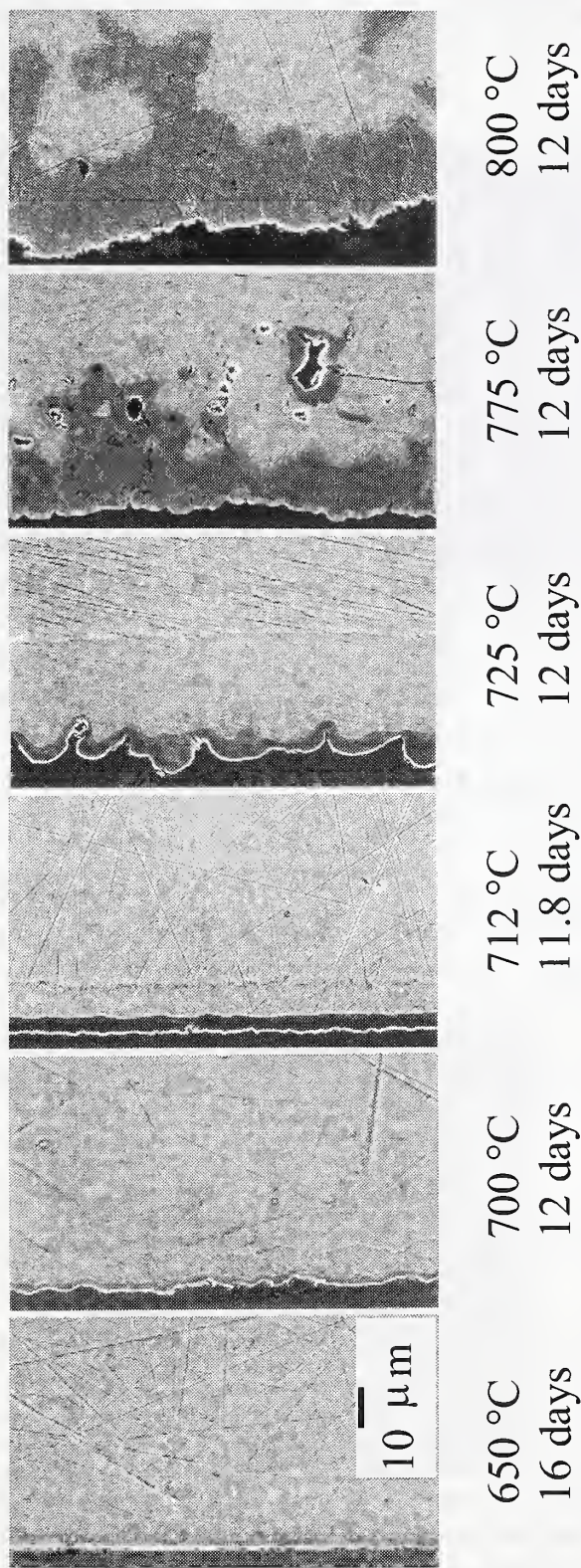
Figure 14. Surface morphology sequence of nuclear grade zirconium exposed to zinc vapor at 650 °C, 700 °C, 712 °C, 725 °C, 775 °C and 800 °C. The black edge along the extreme left side of the micrographs is not part of the sample.

650 °C   700 °C   712 °C   725 °C   775 °C   800 °C
16 days   12 days   11.8 days 12 days   12 days   12 days

10 µm

Micrographs of the reaction layer of the Zircaloy-4 samples heat treated at 650 °C, 670 °C, 700 °C and 725 °C are shown in Figure 15.

| 650 °C | 670 °C | 700 °C | 725 °C |
| 16 days | 21 days | 10 days | 11.8 days |
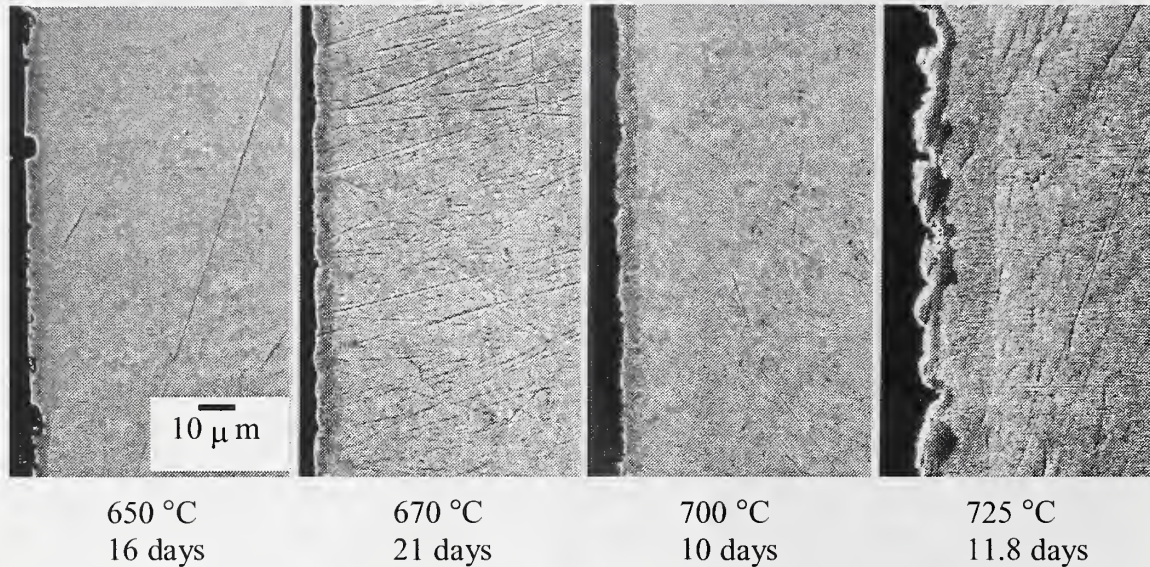
Figure 15. Surface morphology sequence of Zircaloy-4 exposed to zinc vapor at 650 °C, 670 °C, 700 °C and 725 °C. The black edge along the extreme left side of the micrographs is not part of the sample.

The 725 °C Zircaloy-4 sample begins to exhibit this wavy surface phase morphology but it is not as pronounced as the nuclear grade zirconium sample at the same temperature. The phase sequence of the 725 °C sample changes. The dark edge phase is ZnZr and the next layer is the β phase and then the bulk α-Zr. Again one explanation for this change from planar layers at lower temperatures to non-planar may be related to the presence of the β phase at 725 °C.

6.3   TEM of Nuclear Grade Zirconium at 800 °C

At 725 °C , below the reported eutectoid temperature of 750 °C, a β phase containing approximately 85 at. % zirconium was observed. This same β phase was found in nuclear grade zirconium samples heat treated at 775 °C and 800 °C for 12 d. The 800 °C sample had the largest β phase thickness of approximately 450 μm, so this sample was chosen for transmission electron microscope (TEM) analysis. First the sample was ground with 600 grit SiC paper from both sides to remove the ZnZr and α-Zr from the surfaces. Then the sample was jet-electropolished with 5% perchloric and 95% ethanol with 35 V at a temperature of minus 5 °C. TEM analysis confirmed a martensitically transformed bcc structure. Figure 16 a) shows SEM backscattered image of the

martensitic structure on the electropolished surface and b) shows the TEM bright field image of the martensite with different orientations of plate-like variants of α-Zr. None of the samples below 725 °C contain the β phase, see Table 6. Thus at the temperature of the diffusion experiment the phase was bcc.
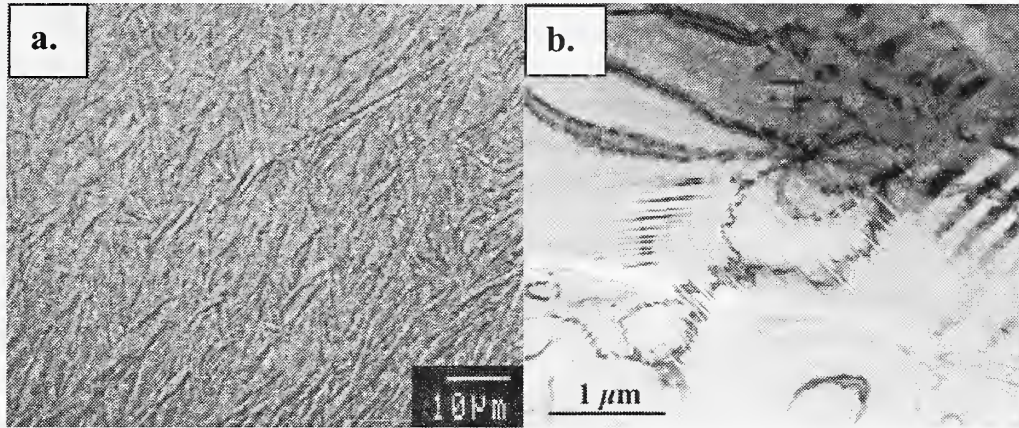
Figure 16. Nuclear grade zirconium heat treated with zinc vapor at 800 °C a) SEM backscattered image of the martensitic structure, b) TEM bright field image of the martensite with different orientations of the plate-like variants of α-Zr.

In Figure 17 two selected TEM diffraction patterns a and b are from the large area of multiple variants from Figure 16b showing in a) pseudo 3-fold symmetry with outlines of hcp reciprocal lattices drawn over the pattern and in b) pseudo 4-fold symmetry clearly corresponding to the parent bcc cubic phase.
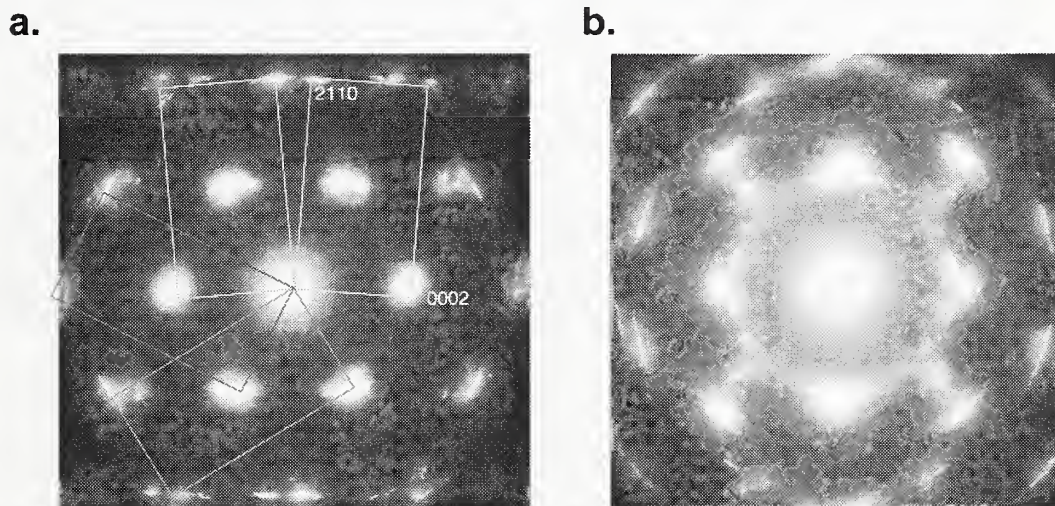
Figure 17. TEM diffraction patterns a and b are from the large area of multiple variants in Figure 16b of nuclear grade zirconium exposed to zinc vapor at 800 °C for 12 d a) 3-fold symmetry and in b) 4-fold symmetry.

6.4   Correction of Eutectoid Temperature

Compositional line scans of nuclear grade zirconium exposed to zinc vapor at 712 °C, 725 °C, 775 °C and 800 °C are shown in Appendix A, Figures A13, A15, A20 and A21, respectively. The β phase was not present at 712 °C, but was present at 725 °C, 775 °C and 800 °C. The β phase, represented by a line with constant slope, ranges from 85 to 88 at. % Zr at 725 °C, 83.5 to 93 at.% Zr at 775 °C, and 82 to 95 at.% Zr at 800 °C. The endpoints from each these sloping lines determine the experimentally obtained phase boundaries of the left and right sides of the β region above the eutectoid temperature in the Zn-Zr phase diagram. Figure 18 shows these experimental data points plotted with the currently reported phase diagram in the region between 70 at.% Zr to 100 at.% Zr [6]. The experimental results predict the eutectoid reaction temperature should be between 712 °C and 725 °C, so the temperature 718 °C was chosen as an estimate.
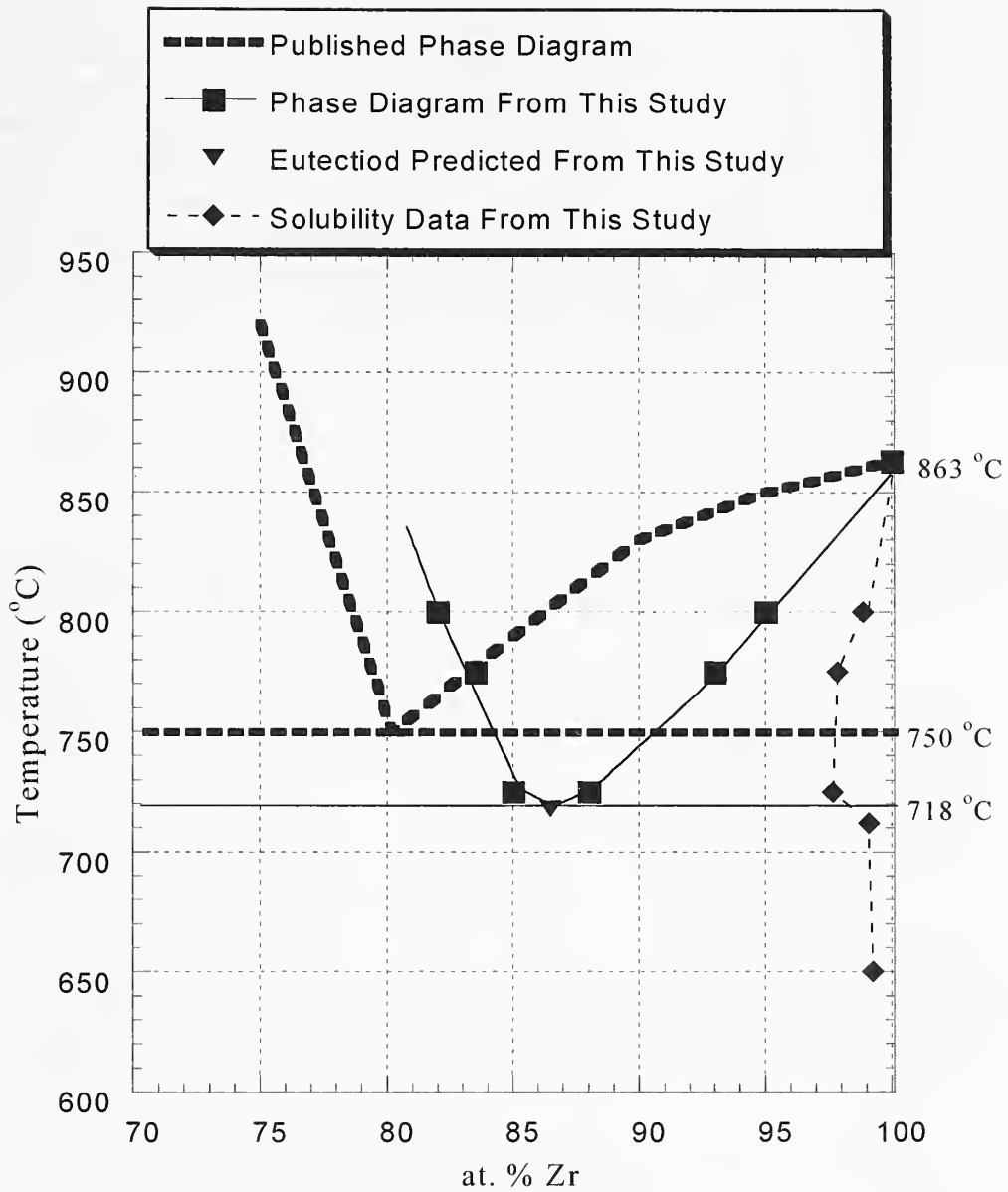
Figure 18. Experimental data from this study is plotted with the currently published phase diagram. The experimental eutectoid reaction temperature (uncertainty is discussed in the text on page 56) is 718 °C at 86.5 at. % Zr and the experimental solubility varies from 0.76 at. % Zn at 650 °C to 1.16 at. % Zn at 800 °C.

6.5   Solubility Estimate

Investigation of the nuclear grade zirconium exposed to zinc vapor revealed a solubility of zinc into zirconium. The compositional line scan data of the nuclear grade zirconium samples was acquired until the amount of zinc in the zirconium reached zero and remained zero for approximately 5 μm. The total depth of zinc penetration into the nuclear grade zirconium is reported in Table 11. The reported uncertainties in Table 11 are absolute bounds errors. The solubility limits were determined by extrapolating the measured values to the interface position. This data is shown in Table 11 and plotted in Figure 18, in the previous section.

Table 11 Solubility Data of Zinc into Nuclear Grade Alpha Zirconium

NGZR				
Temperature (°C)	Time (d)	Total Reaction Zone Thickness (μm) ± 0.5 μm	Penetration Depth of Zinc into the Alpha Zirconium (μm)	Solubility of Zn in α-Zr (at. % Zn) ± 0.3 at%
650	16	3.0	18.0	0.76
	64	6.0	34.0	NM
700	12	3.2	≈30.0	NM
	32	6.3	≈70.0	NM
712	11.8	3.5	35.0	0.92
725	11.8	51.0	82.0	2.4
	64	205.0	265.0	NM
775	12	287.0	≈300.0	2.2
800	12	450.0	465.0	1.2

NM = NOT MEASURED

6.6 ZnZr$_2$ Phase

The ZnZr$_2$ phase was only observed between the temperatures of 712 °C and 725 °C. Diffusion couples at 775 °C and 800 °C did not contain this phase, and in diffusion couples below 712 °C this phase was not present. Assuming no nucleation barriers this would suggest a phase diagram of the type shown in Figure 19. A peritectoid reaction of β + ZnZr $\rightarrow$ ZnZr$_2$ and a eutectoid reaction of ZnZr$_2$ $\rightarrow$ ZnZr + α-Zr would lie somewhere between 712 °C and 725 °C. However, this temperature range could be larger, possibly from just above 700 °C to just below 775 °C. Another interpretation is

that the $ZnZr_2$ fails to nucleate in the low temperature couples and that the $ZnZr_2$ phase does exist at much lower temperatures. Further work needs to be done to confirm the exact temperature range over which the $ZnZr_2$ phase exists.
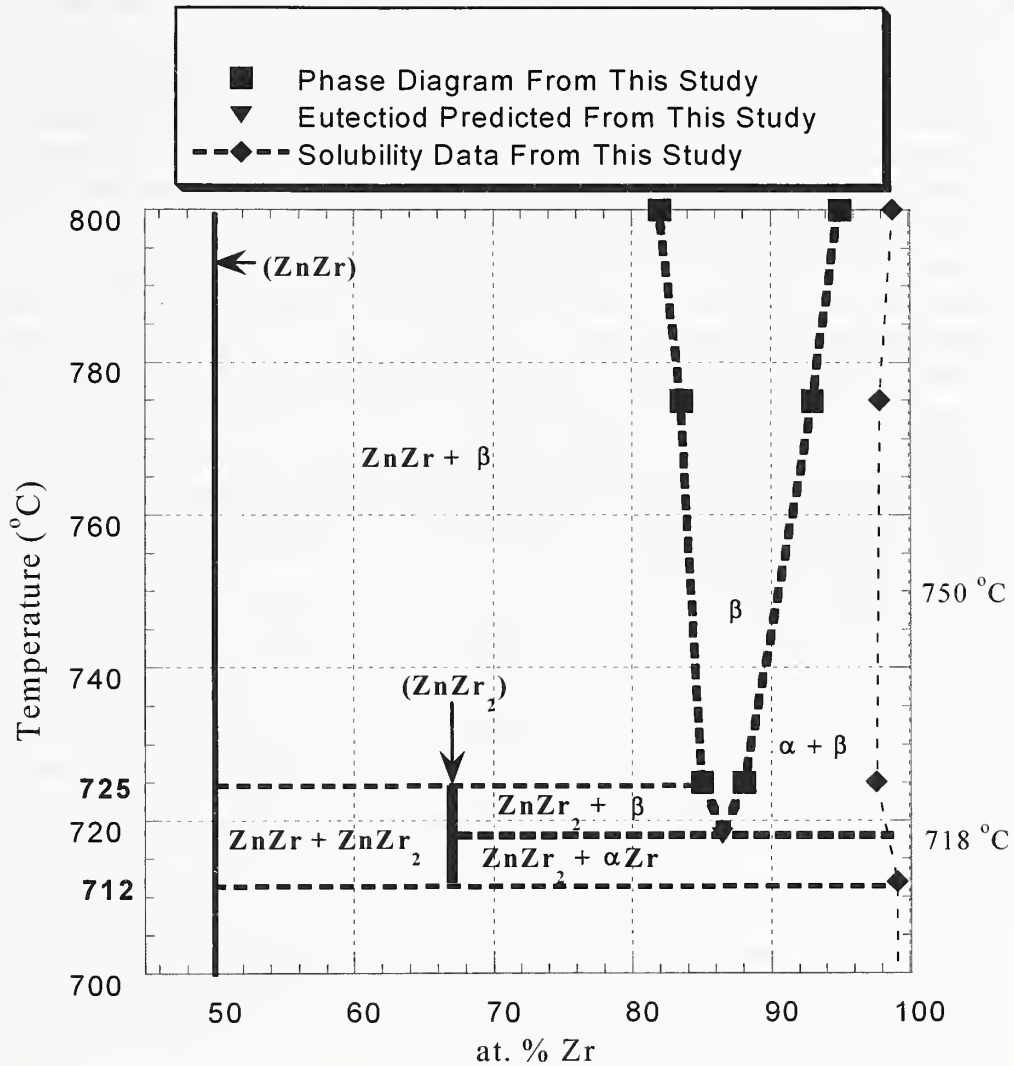
Figure 19. Experimental Zn-Zr phase diagram from this study. 718 °C is the estimated eutectoid temperature (uncertainty is discussed in the text on page 56).

7   CONCLUSIONS

Zircaloy-4 and nuclear grade zirconium were exposed to zinc vapor in the temperature range of 650 °C to 800 °C. The spatial sequence of intermetallic phases from the surface into the interior and the total depth of zinc penetration were measured.

- The Zn_2Zr intermetallic is the surface phase to form in these diffusion experiments with α-brass as the zinc vapor source even though four other intermetallics with higher zinc content are listed Table 1. The likely reason Zn_2Zr is the surface phase rather than a more zinc rich phase may be due to the activity of the zinc in the α-brass being lower than the activity of pure zinc.
- Fe and Sn alloying elements in Zircaloy-4 substitute on the Zn sublattice in the $ZnZr_2$ and $ZnZr$ phases: $(Zn, Fe, Sn)Zr_2$ and $(Zn, Fe, Sn)Zr$. Fe and Sn are insoluble in the Zn_2Zr phase and the α-Zr.
- A two phase layer of $(Zn,x)Zr_2 + (Zn,x)Zr$ is present in all of the Zircaloy-4 TREX samples in the temperature range of 650 °C to 725 °C.
- The eutectoid temperature was found to be lower than the currently reported temperature of 750 °C in the literature. This research puts the eutectoid reaction temperature at approximately 718 °C (± 6 °C absolute bounds error) with a composition of 86.5 at. % Zr.
- The solubility of zinc in nuclear grade α-zirconium was measured from the composition line scan profiles at five different temperatures. The solubility of zinc increased with temperature from 0.76 at. % Zn at 650 °C to a maximum of 2.36 at. % Zn at 725 °C and decreased with further increases in temperature up to 800 °C.
- The growth constant K for total zinc penetration in both Zircaloy-4 and nuclear grade zirconium samples at 650 °C, 700 °C, and 725 °C for various times confirmed parabolic growth. The activation energy, Q, for Zircaloy-4 below 725 °C was measured as 128.56 kJ/mole, and the activation energy of nuclear grade zirconium below 725 °C was measured as 126.65 kJ/mole. The close agreement in activation energy between the nuclear grade zirconium and Zircaloy-4 would be expected since Zircaloy-4 is a dilute zirconium alloy. However, for nuclear grade zirconium at 725 °C and above, containing the β phase, the activation energy for the total zinc penetration is 554.69 kJ/mole.
- The intermetallic $ZnZr_2$ phase was observed between the temperatures of 712 °C and 725 °C. A peritectoid reaction of $β + ZnZr \rightarrow ZnZr_2$ and a eutectoid reaction of $ZnZr_2 \rightarrow ZnZr + α-Zr$ lie somewhere between 712 °C and 725 °C.
- Extrapolating from 650 °C to the lower temperature of 350 °C, using the experimentally measured activation energy of 128.56 kJ/mole and the growth constant coefficient K_0 equal to 3.741×10^{-6} for Zircaloy-4, calculations predict there would not be any significant diffusion reaction in 2000 years. However, experimental results from a Zircaloy-4 TREX sample heat treated with pure zinc at 350 °C for 6 months indicate that a significant reaction does occur.

FUTURE DIRECTION OF THIS WORK

Extrapolating from 650 °C to the lower temperature of 350 °C, using the experimentally measured activation energy of 128.56 kJ/mole and the growth constant coefficient K_0 equal to 3.741×10^{-6} for Zircaloy-4, calculations predict there would not be any significant diffusion reaction in 2000 years. An experiment was performed to check the validity of the extrapolation with a Zircaloy-4 TREX sample heat treated with pure zinc at 350 °C for 6 months and a significant reaction does occur. This finding implies another mechanism, possibly grain boundary diffusion, may be dominate at the lower temperatures. The results of this high temperature work and the single low temperature experiment has prompted the NRC to request an additional investigation into the reactions caused by zinc vapor.

Further experiments with pure zinc at temperatures 400 °C and below will be performed with Zircaloy-4 tubing that has been oxidized, Zircaloy-4 tubing with a reduced wall thickness, Zircaloy-4 TREX as-received, and nuclear grade zirconium as-received. The pre-oxidized tubing, with approximately 100 μm zirconium oxide layer, simulates the end of life oxidation typically observed on cladding after 5 years service in a reactor core. The tubing with a wall thickness reduced to ½ the original wall thickness will be used as mechanical test specimens to investigate the possible grain boundary migration of zinc. The Zircaloy-4 TREX as-received and the nuclear grade zirconium as-received samples will be exposed to zinc vapor to study the phase growth at low temperatures.

APPENDIX
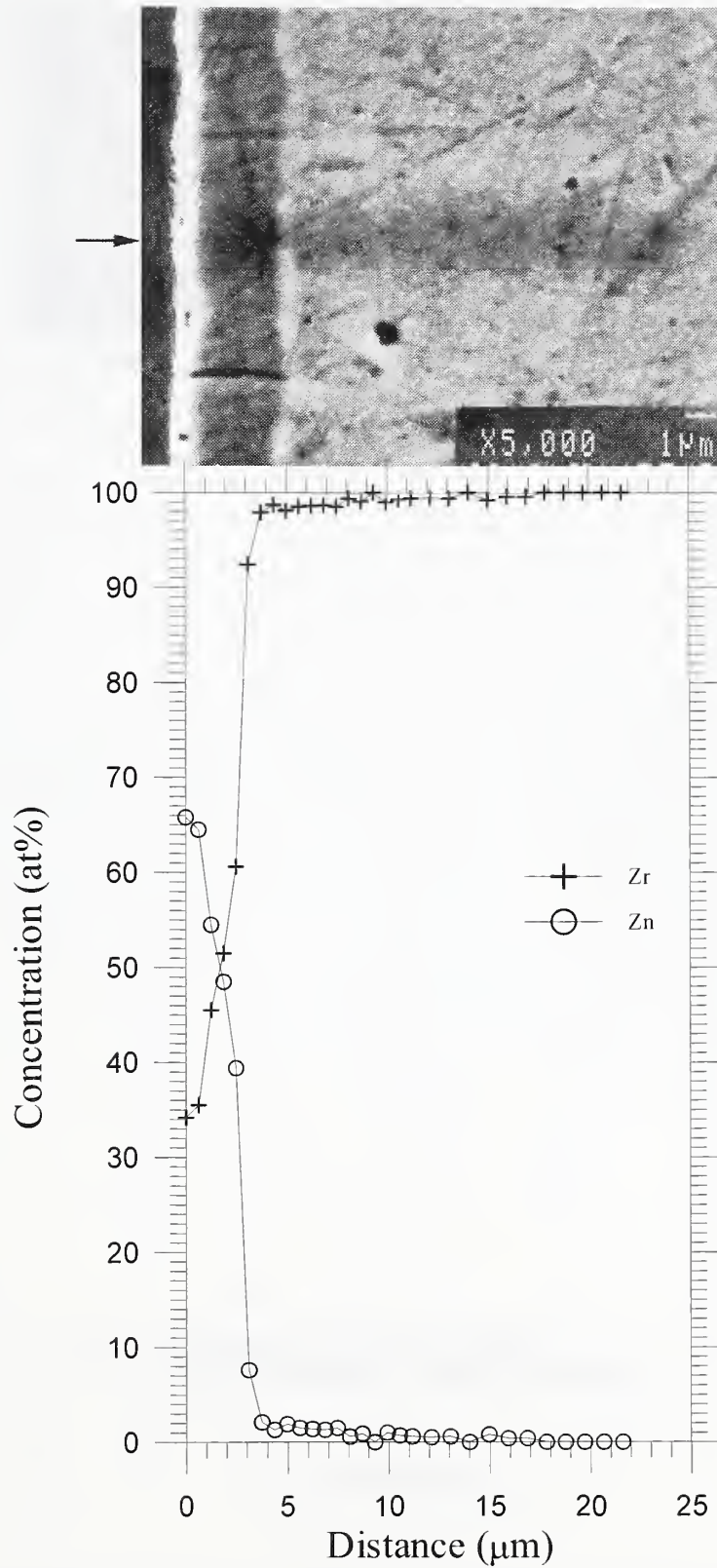
Figure A1. Nuclear grade zirconium heat treated with zinc vapor at
650 °C for 16 d, water quenched.
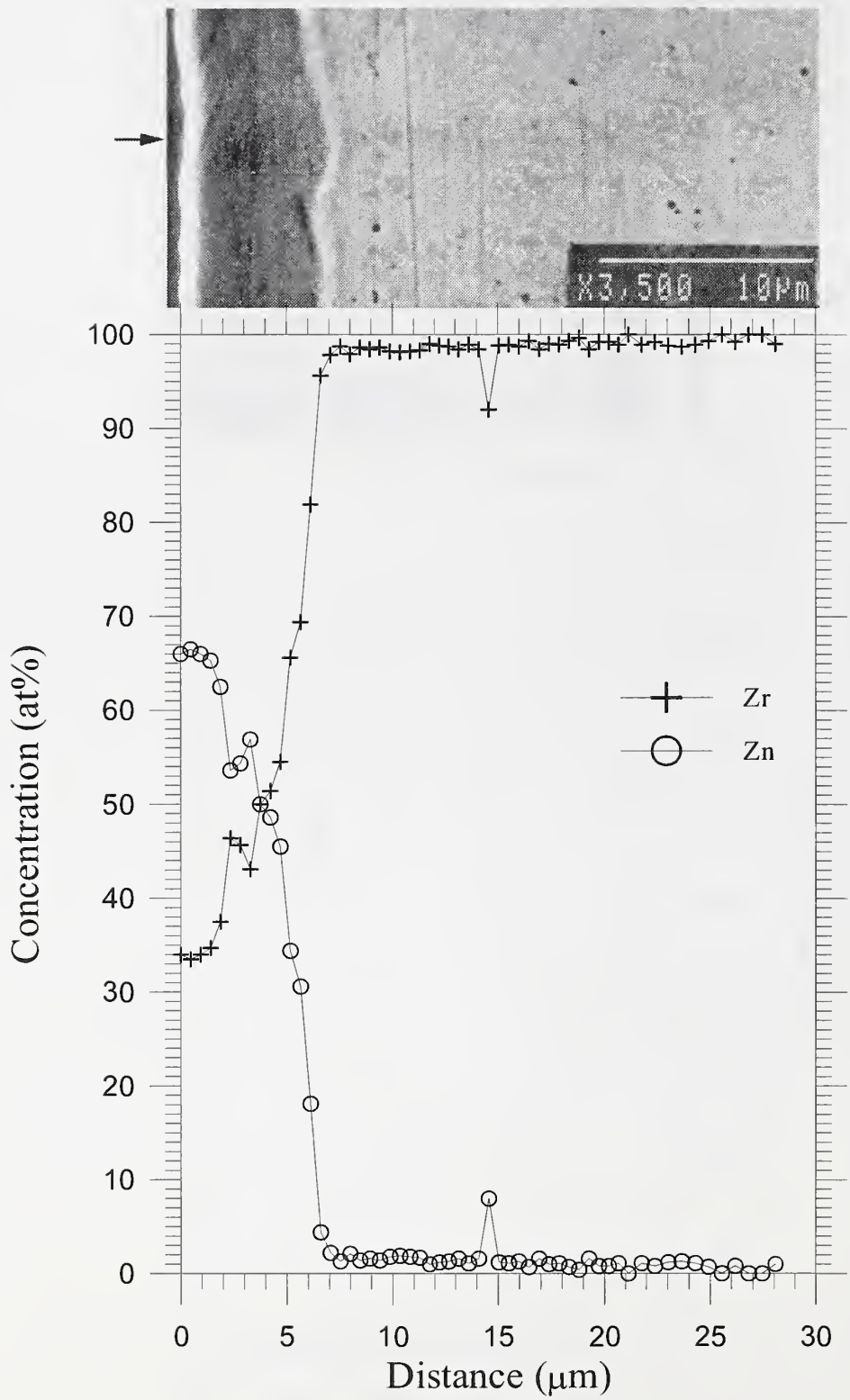
Figure A2. Nuclear grade zirconium heat treated with zinc vapor at
650 °C for 64 d, water quenched.

48
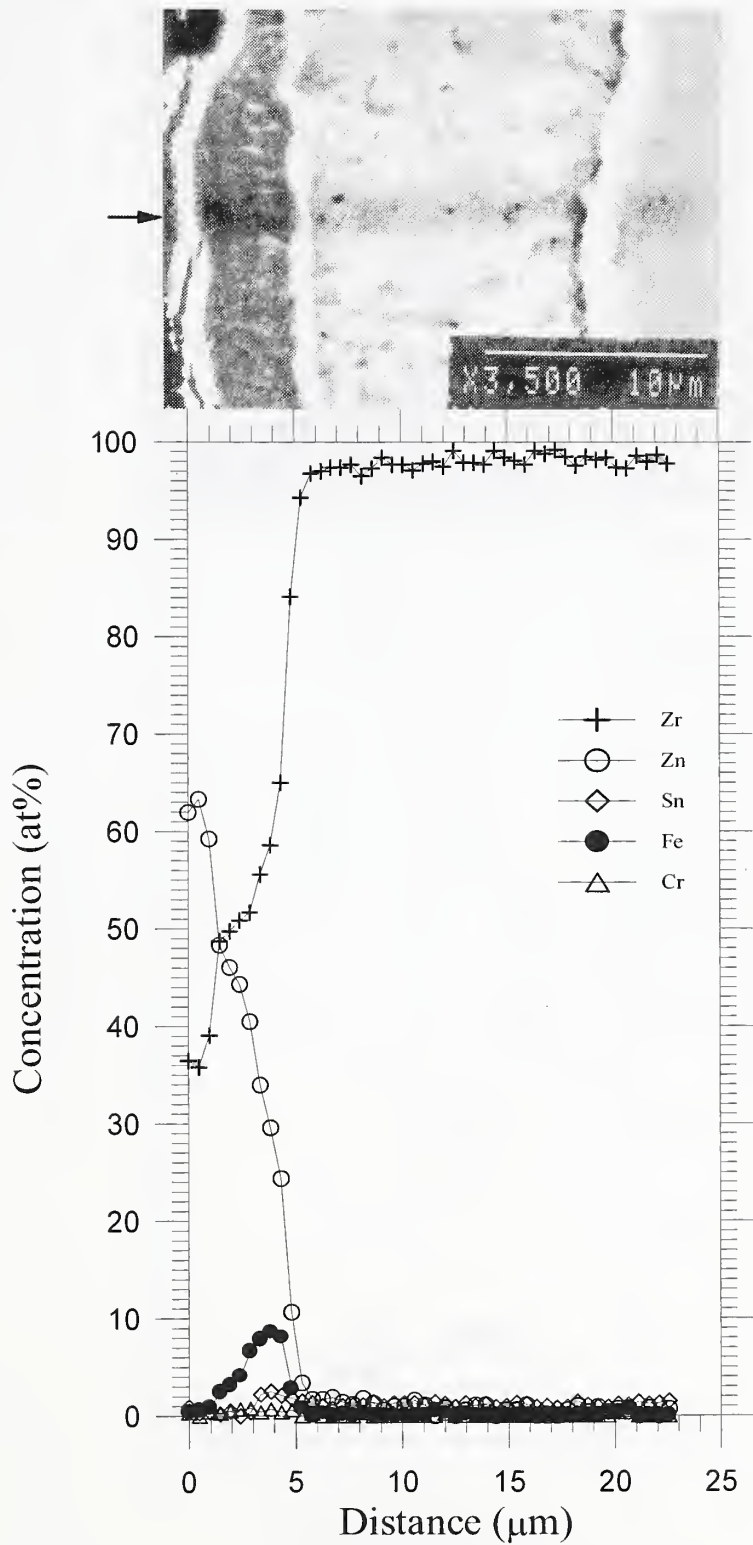
Figure A3. Zircaloy-4 TREX heat treated with zinc vapor at 650 °C for 16 d, water quenched.
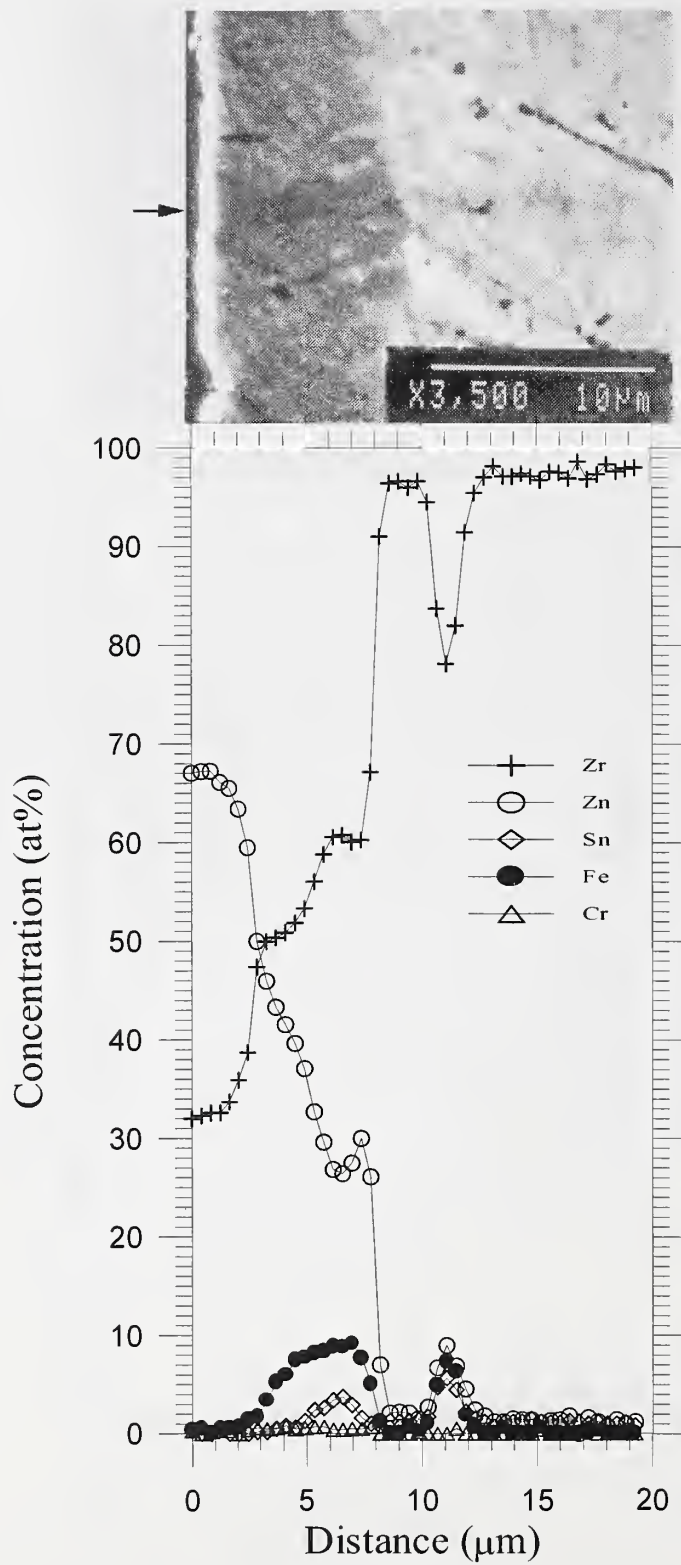
Figure A4. Zircaloy-4 TREX heat treated with zinc vapor at
650 °C for 64 d, water quenched.
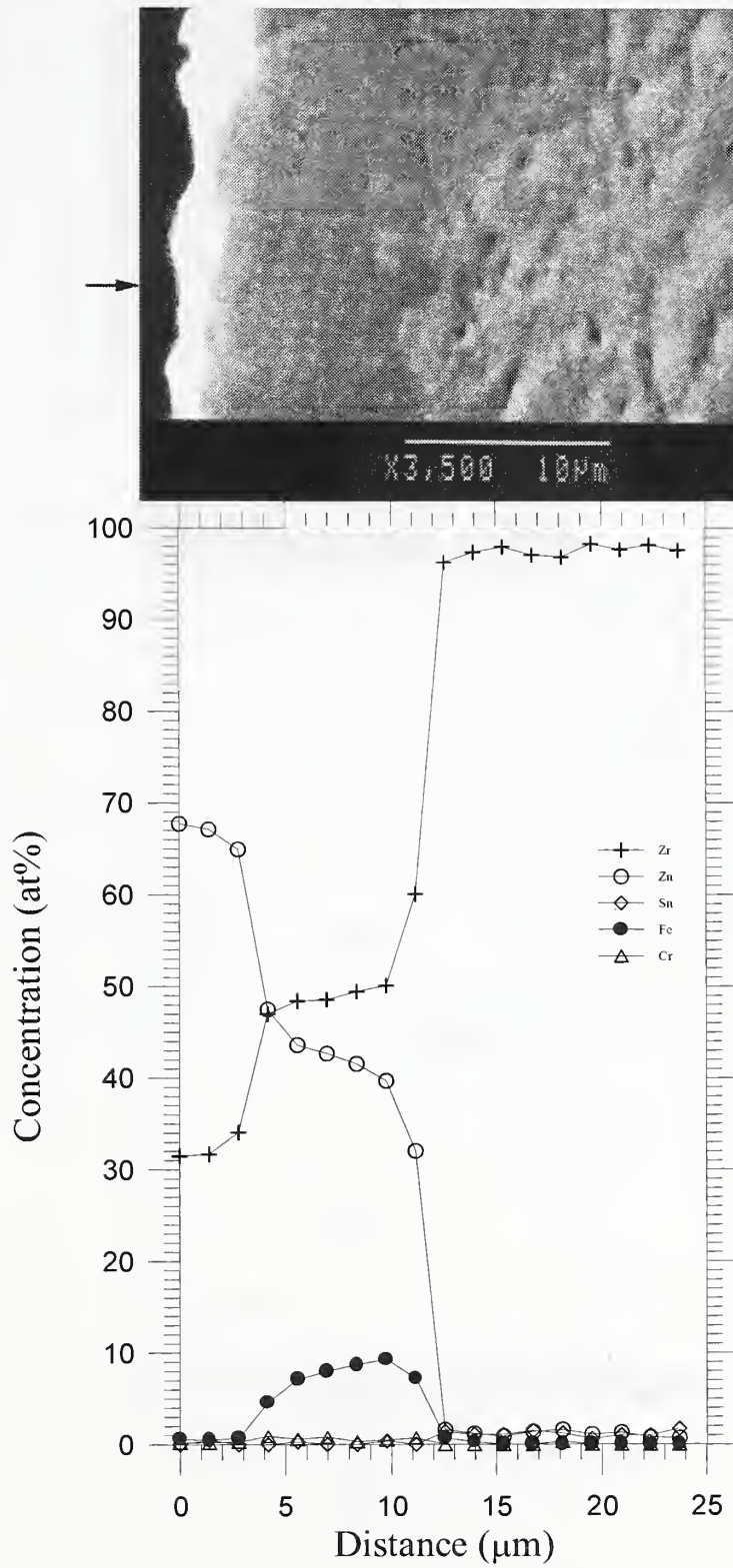
Figure A5. Zircaloy-4 TREX heat treated with zinc vapor at 650 °C for 126 d, water quenched.
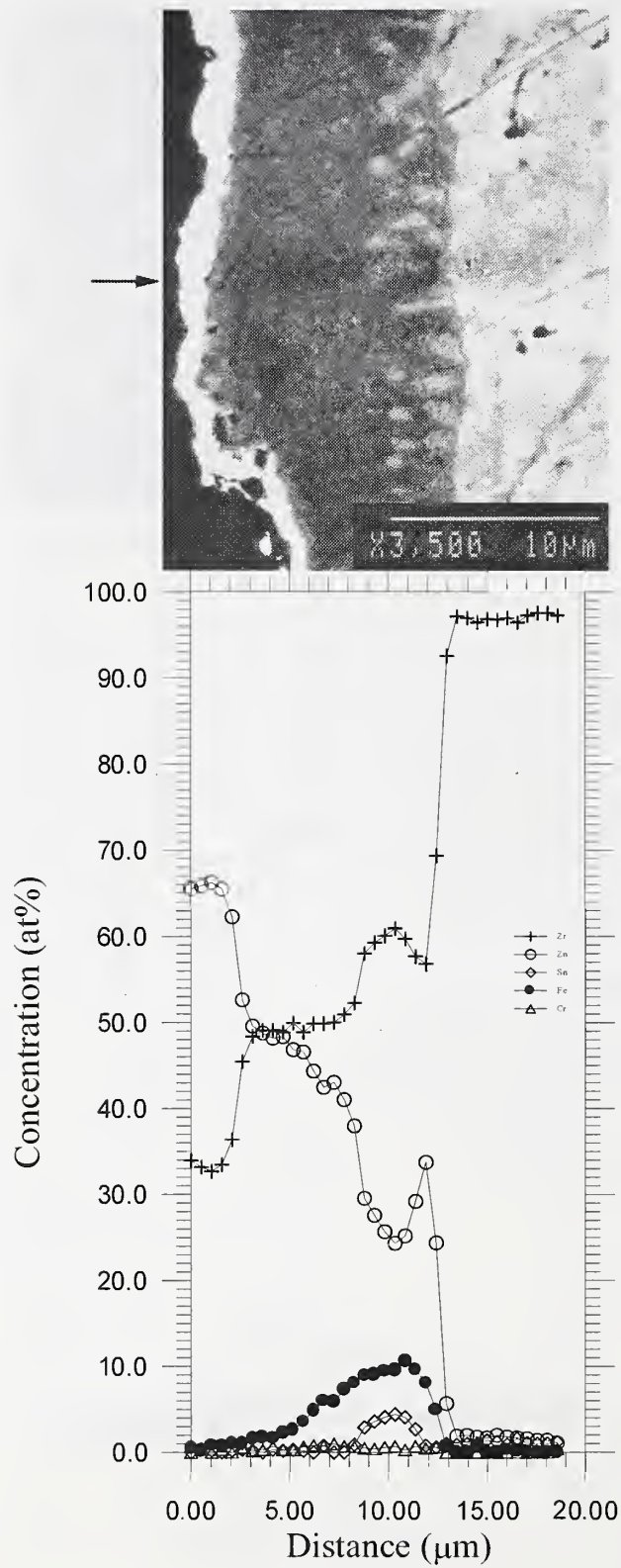
Figure A6. Zircaloy-4 TREX heat treated with zinc vapor at
650 °C for 126 d, water quenched.
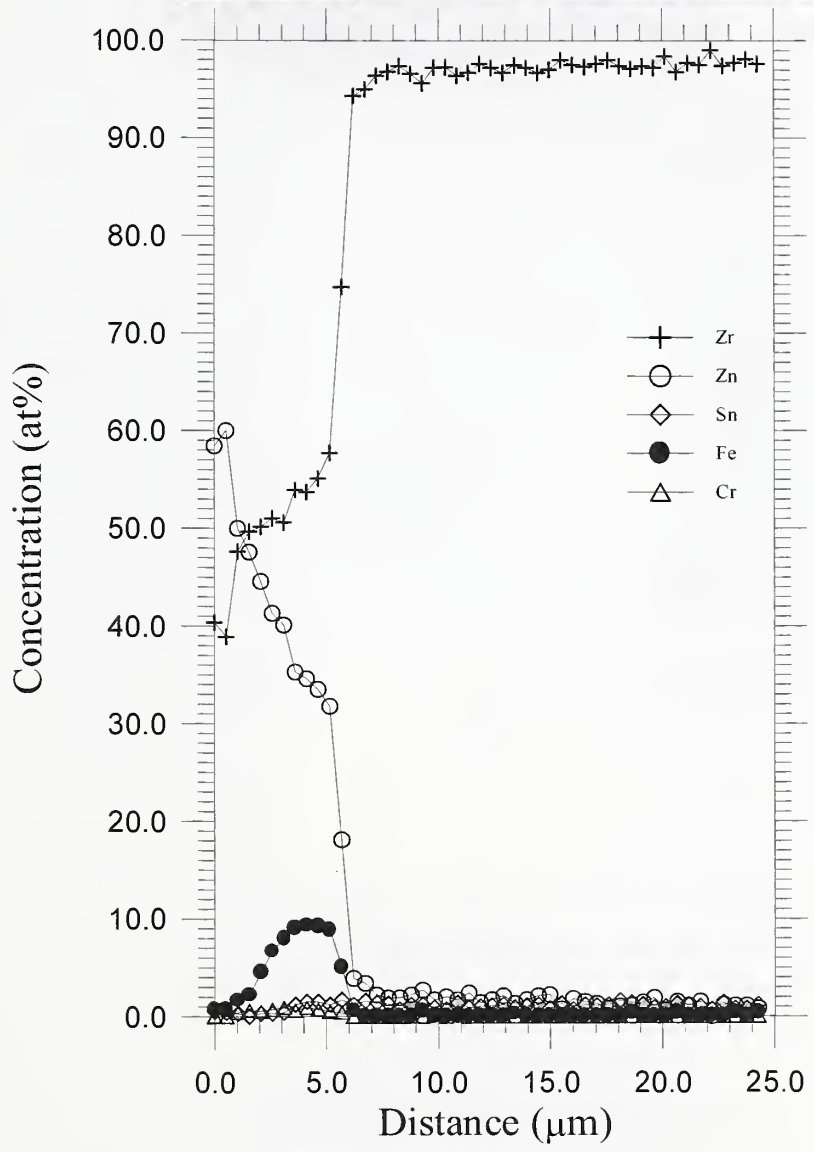
Figure A7. Zircaloy-4 TREX heat treated with zinc vapor at
670 °C for 20.75 d, water quenched.
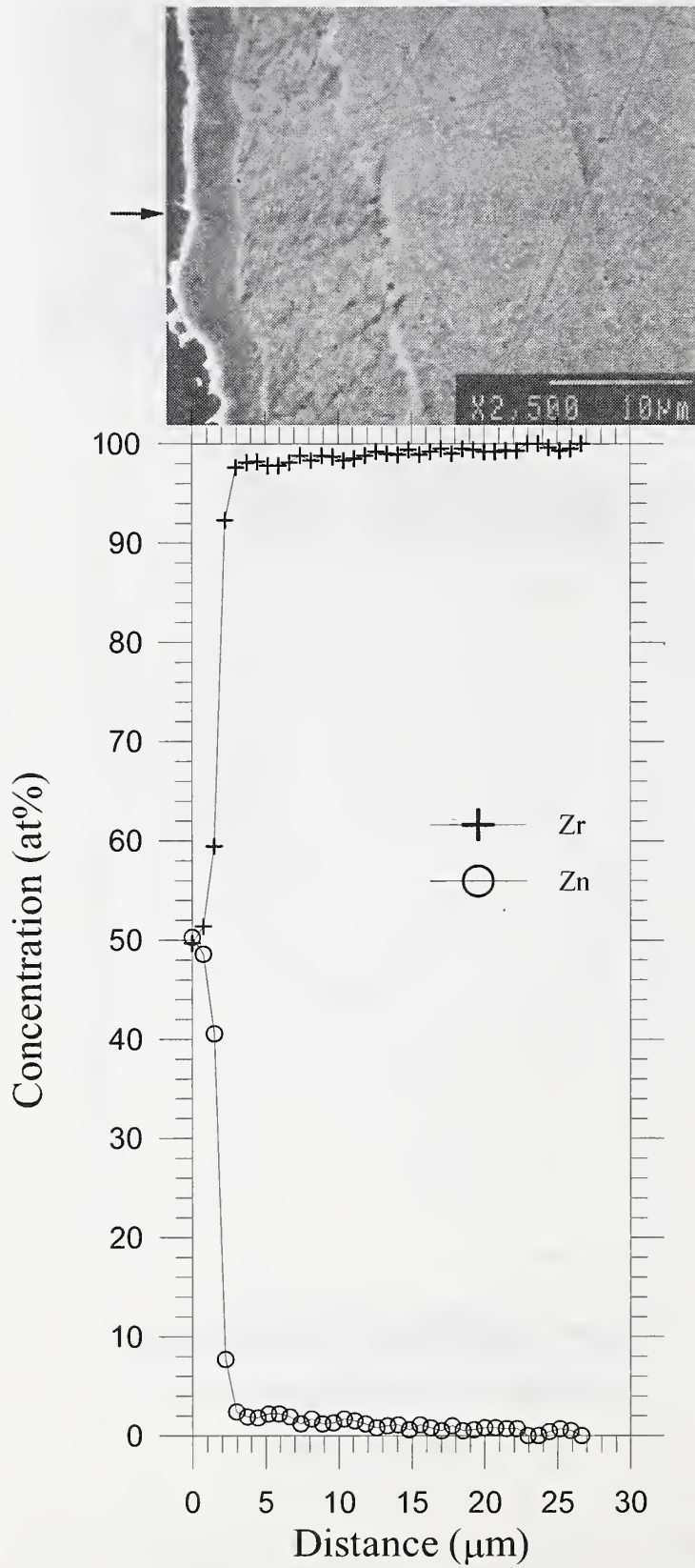
Figure A8. Nuclear grade zirconium heat treated with zinc vapor at 700 °C for 12 d, water quenched.
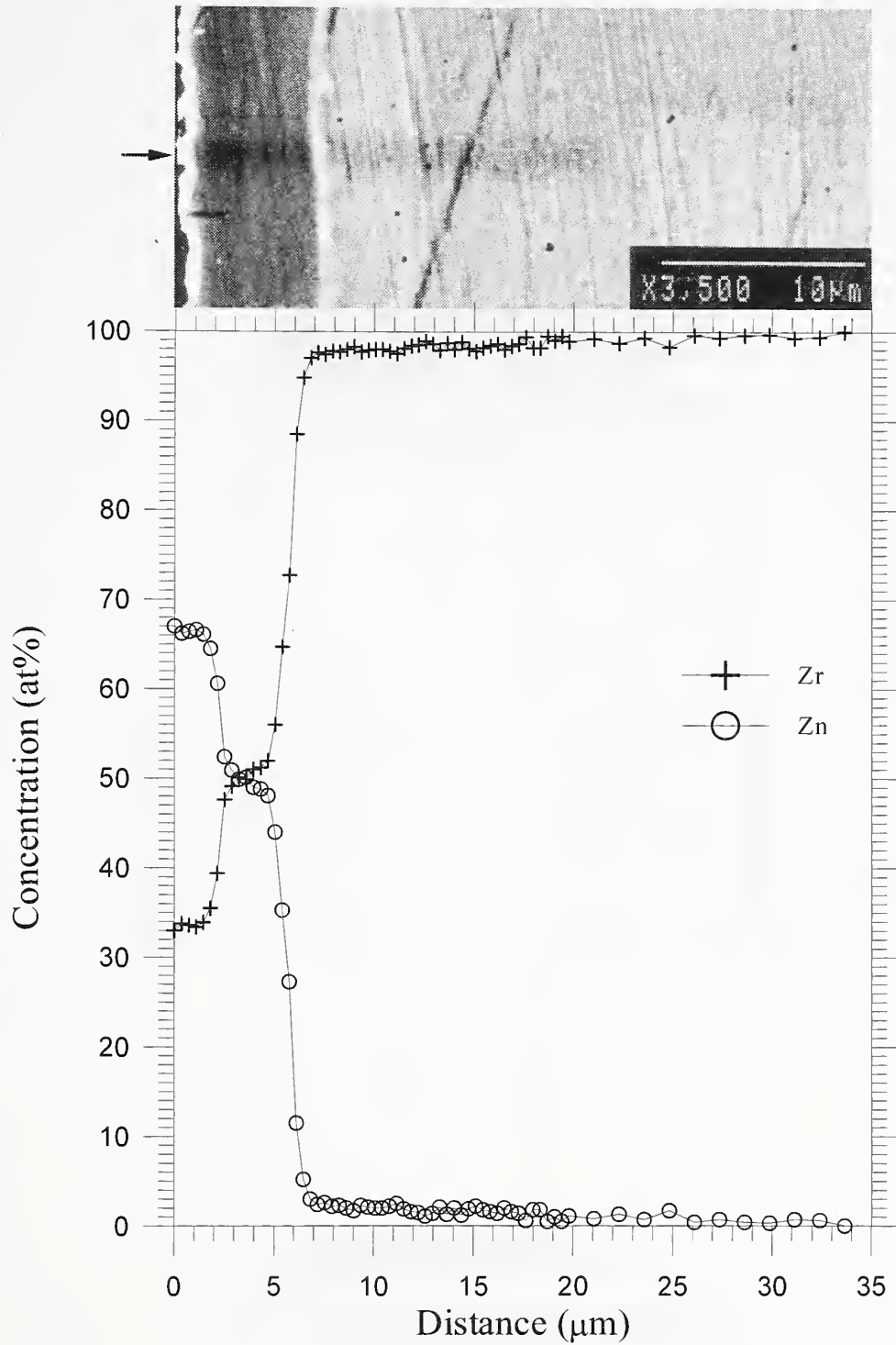
Figure A9. Nuclear grade zirconium heat treated with zinc vapor at 700°C for 32 d, water quenched.
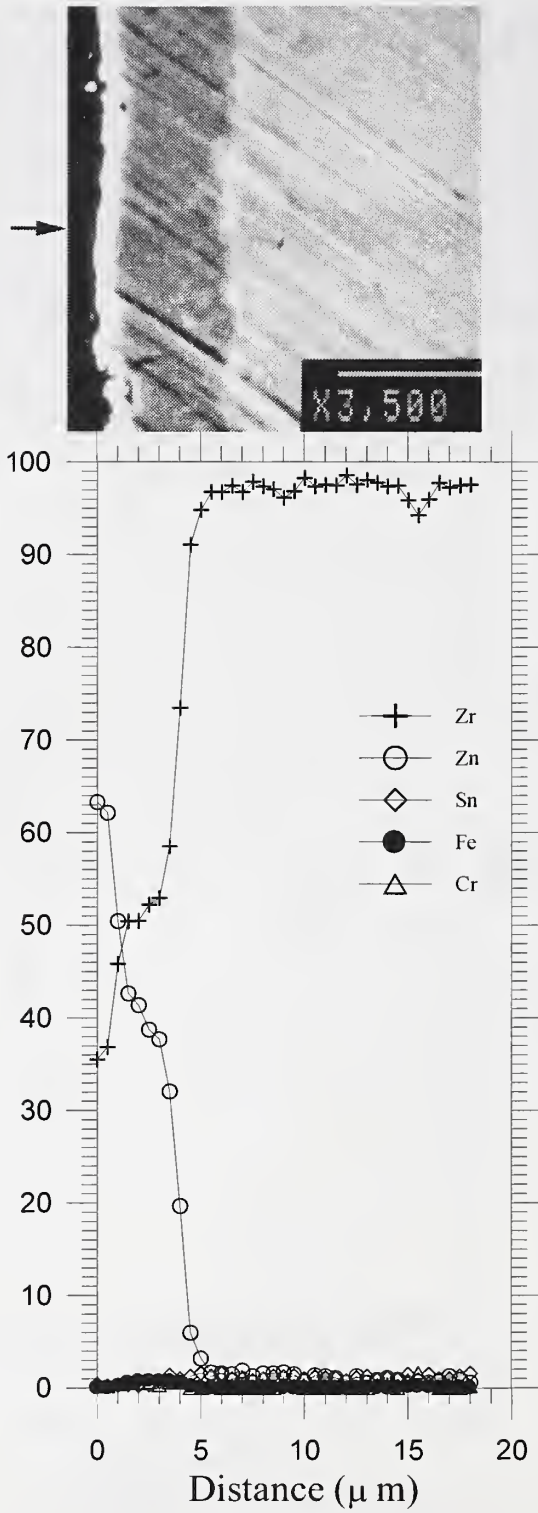
Figure A10. Zircaloy-4 TREX heat treated with zinc vapor at
700 °C for 4 d, water quenched.
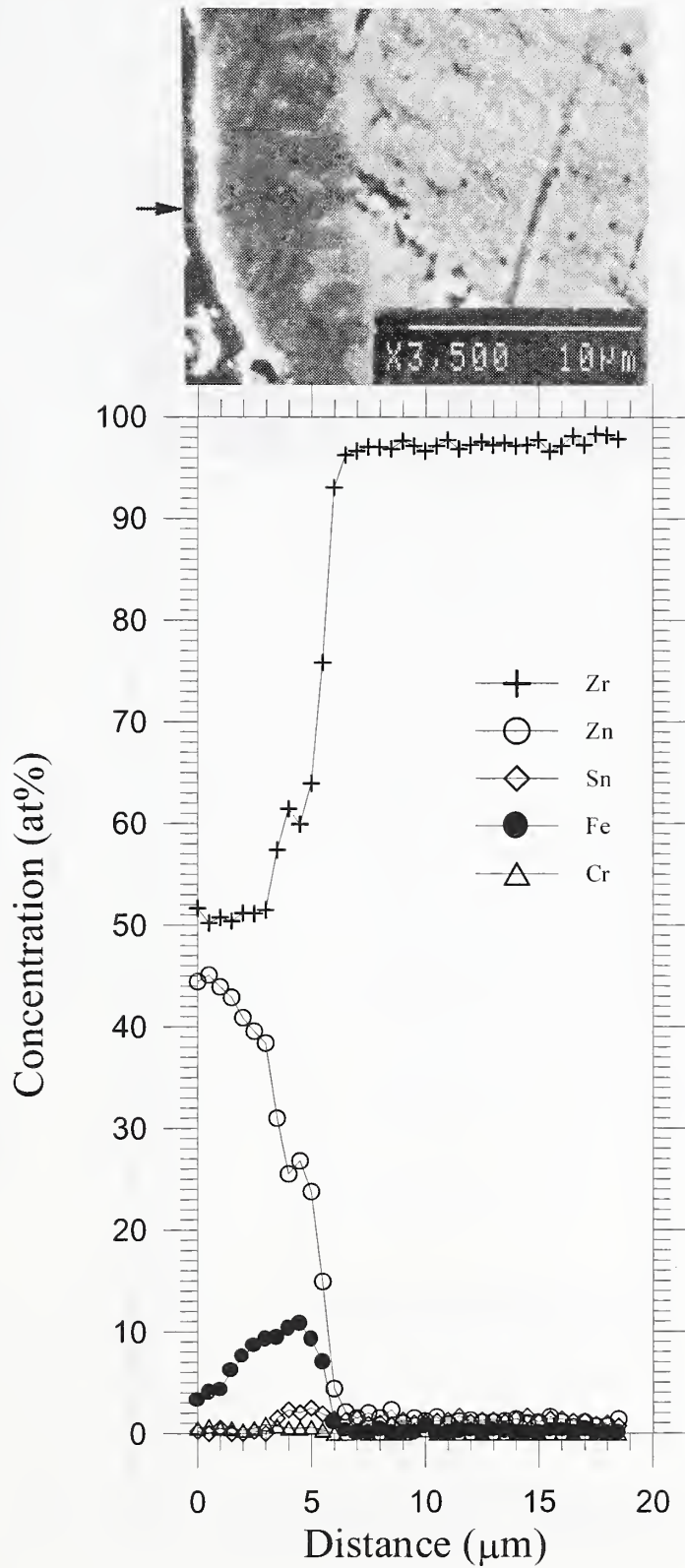
Figure A11. Zircaloy-4 TREX heat treated with zinc vapor at
700 °C for 10 d, water quenched.
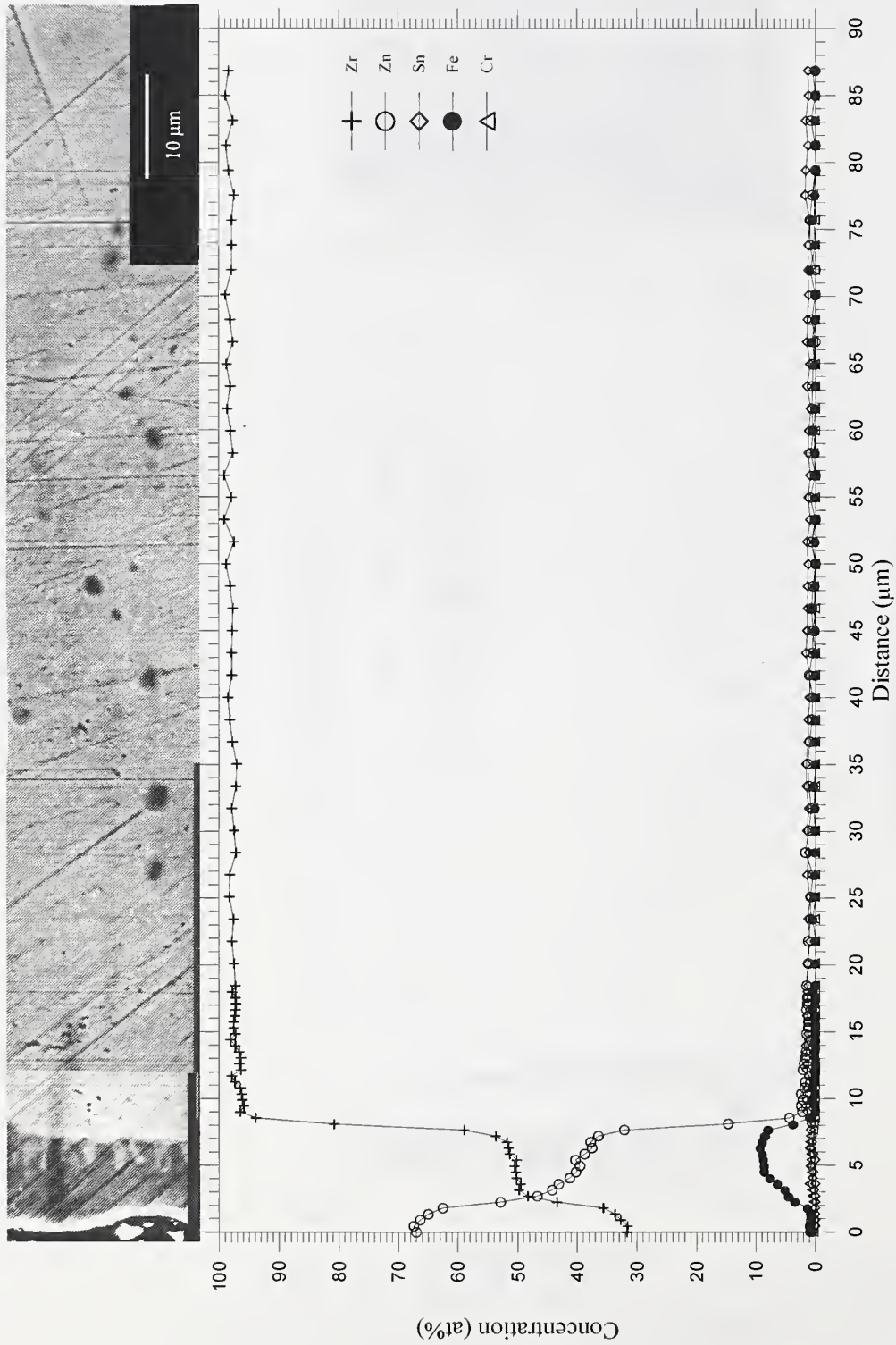
Figure A12. Zircaloy-4 TREX heat treated with zinc vapor at 700 °C for 32 d, water quenched.
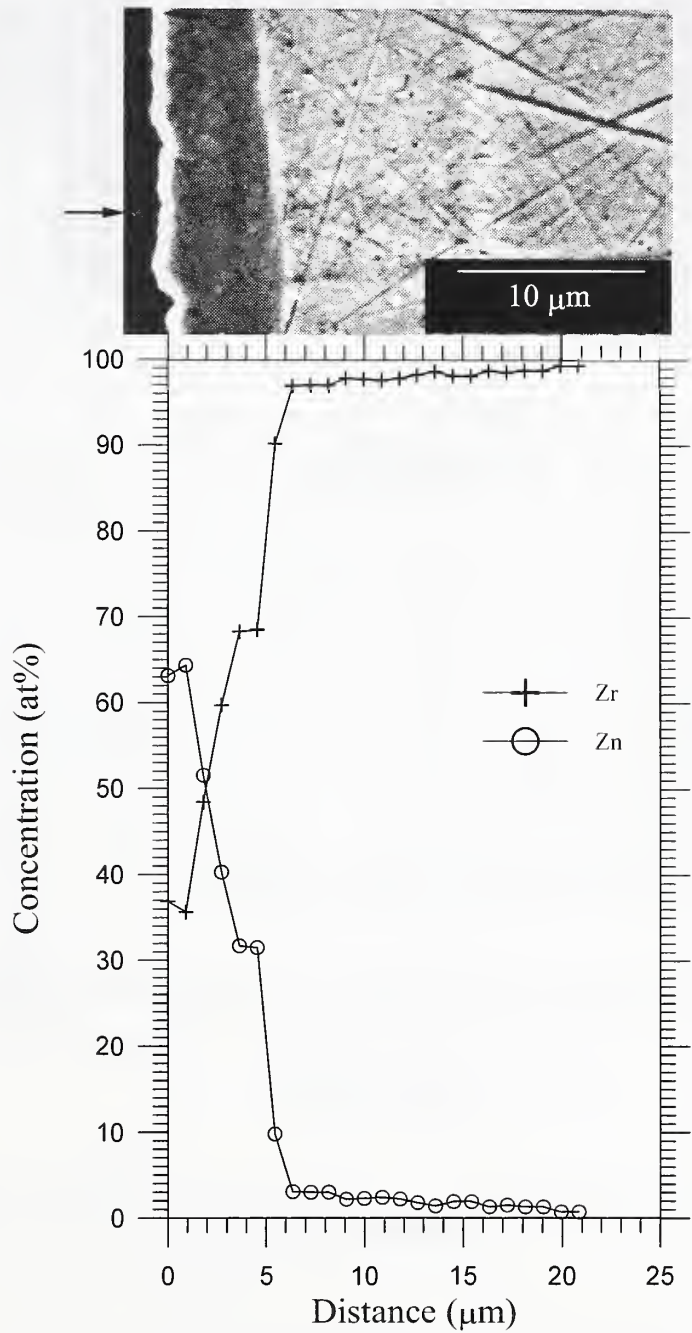
Figure A13. Nuclear grade zirconium heat treated with zinc vapor
at 712 °C for 11.8 days, water quenched.
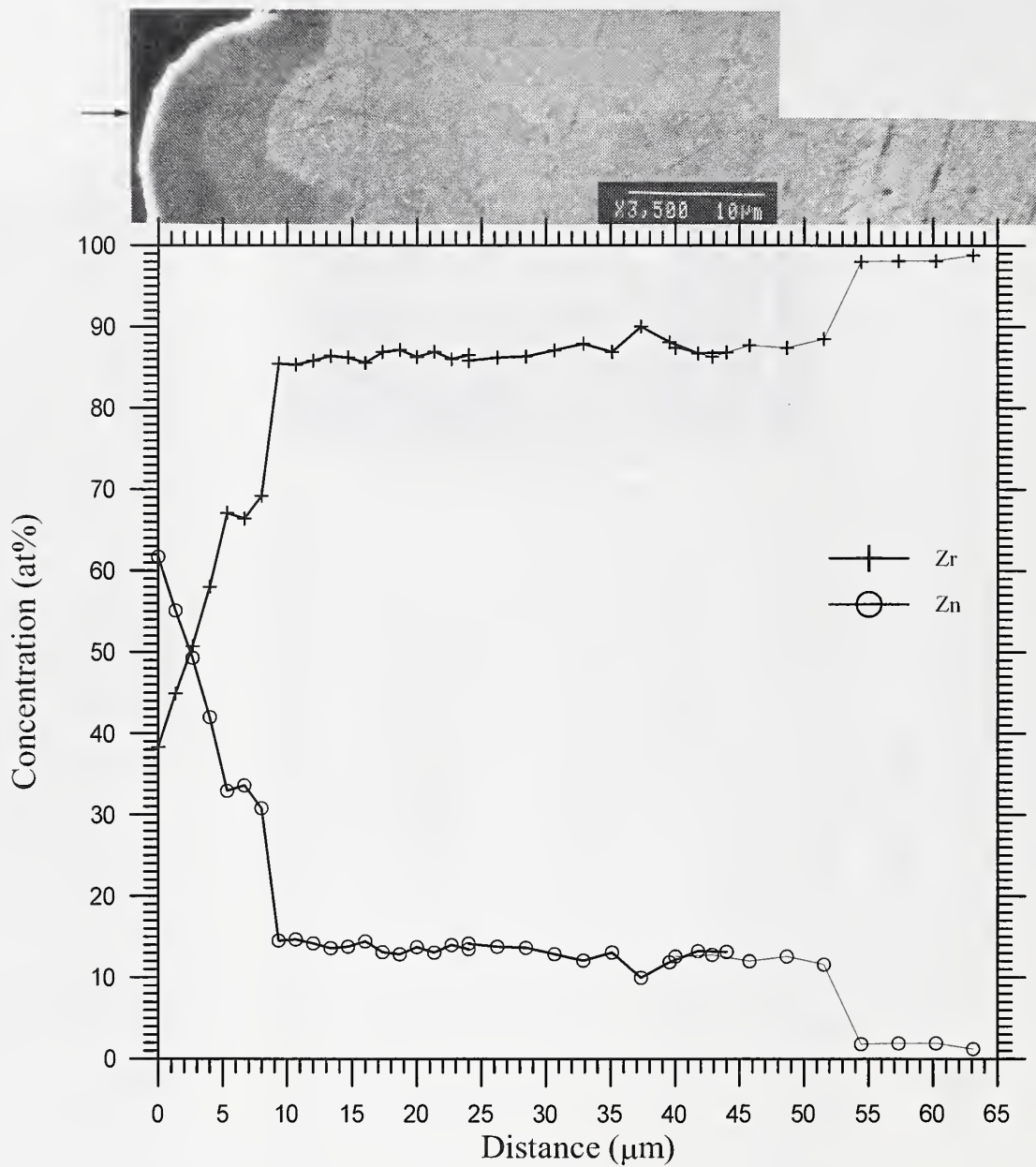
Figure A14. Nuclear grade zirconium heat treated with zinc vapor at 725 °C for 11.8 d, water quenched.
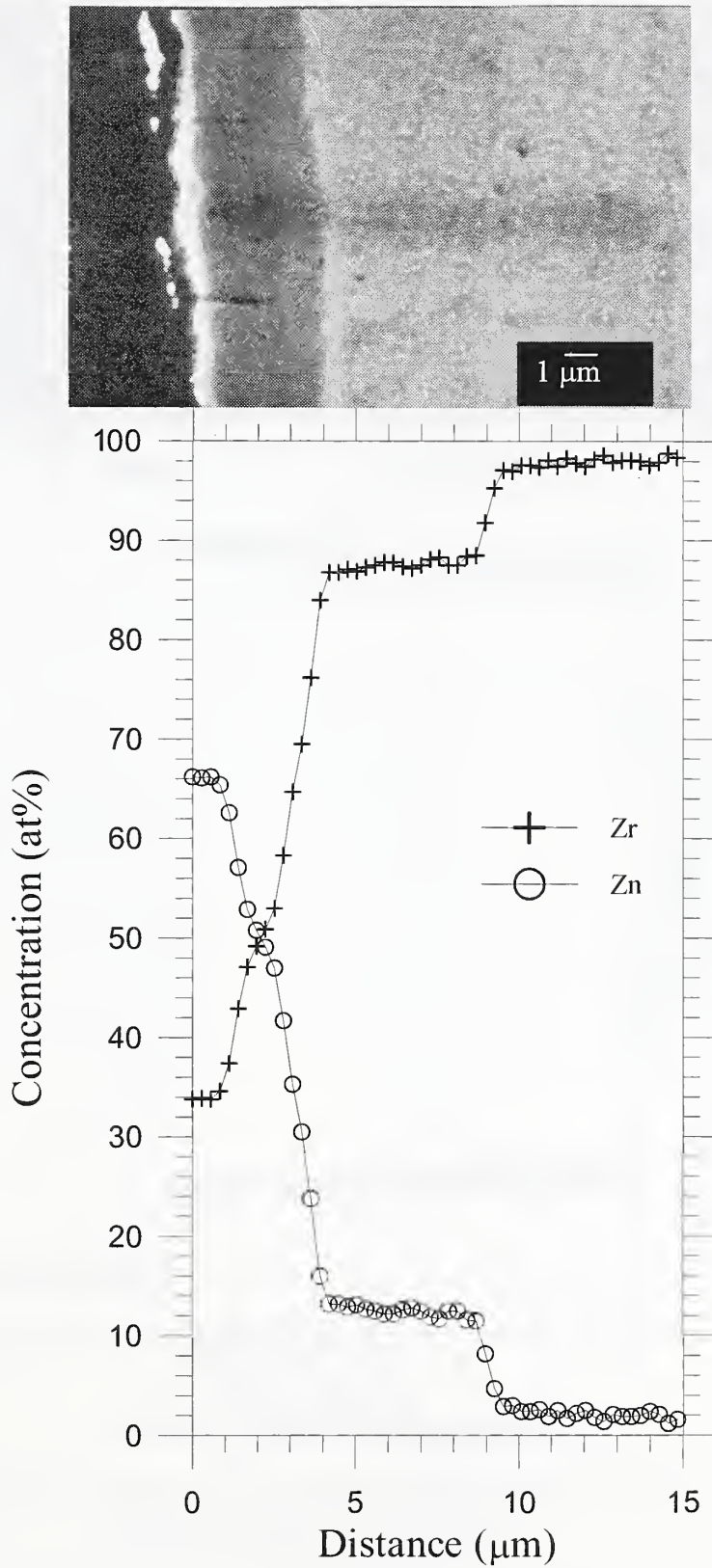
Figure A15. Nuclear grade zirconium heat treated with zinc vapor at
725 °C for 12 d, water quenched.
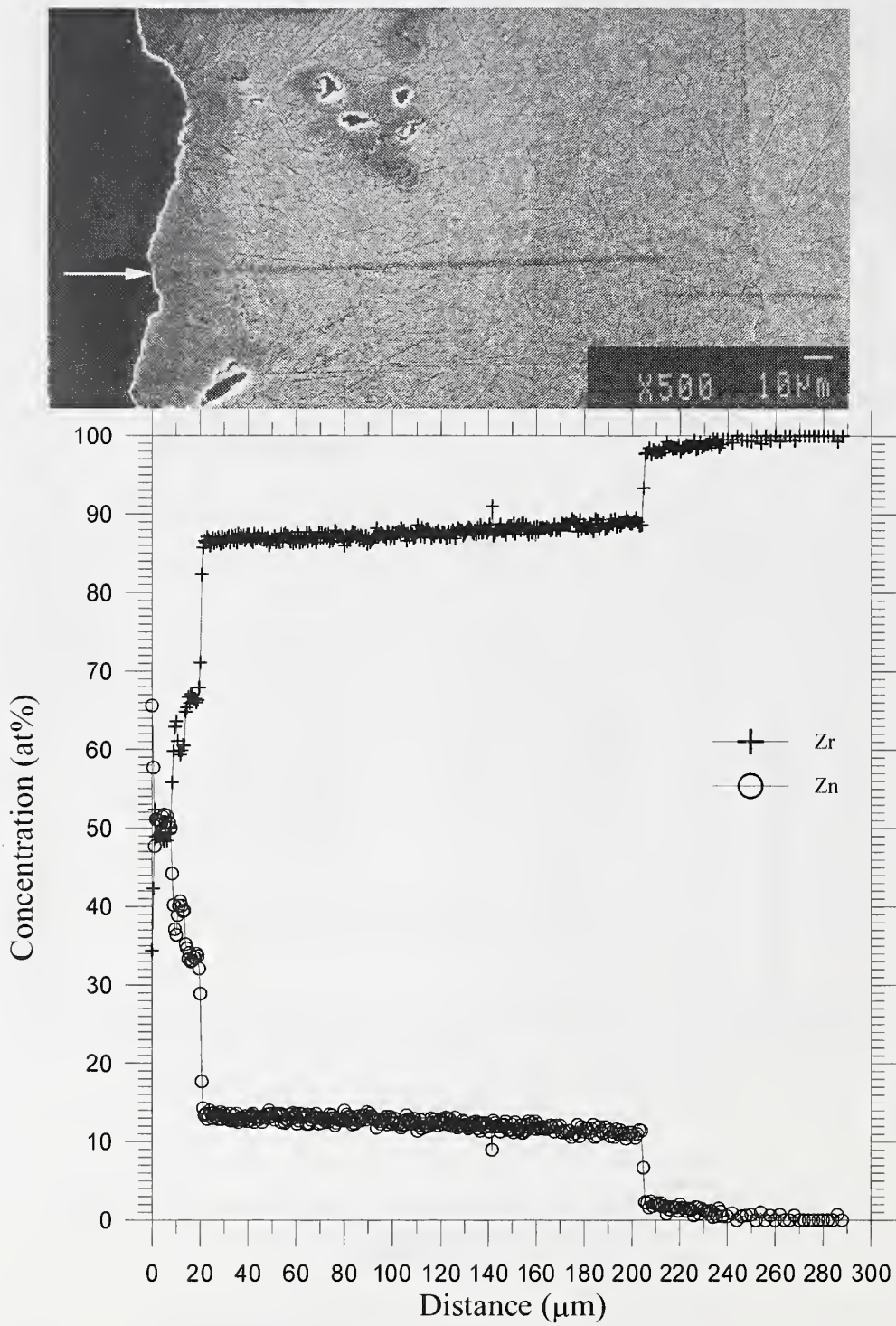
Figure A16. Nuclear grade zirconium heat treated with zinc vapor at 725 °C for 64 d, water quenched.
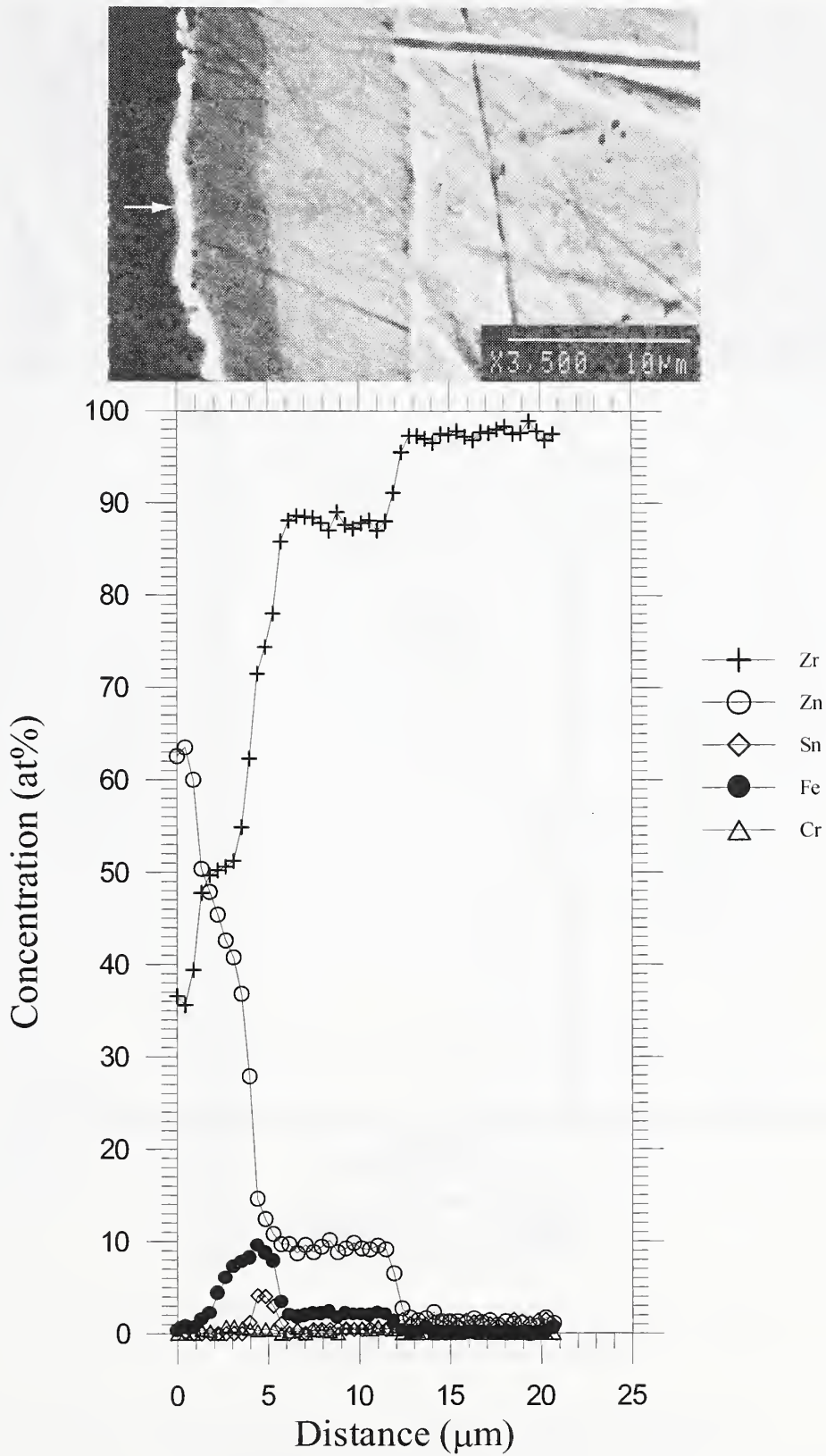
Figure A17. Zircaloy-4 TREX heat treated with zinc vapor at
725 °C for 2 d, water quenched.
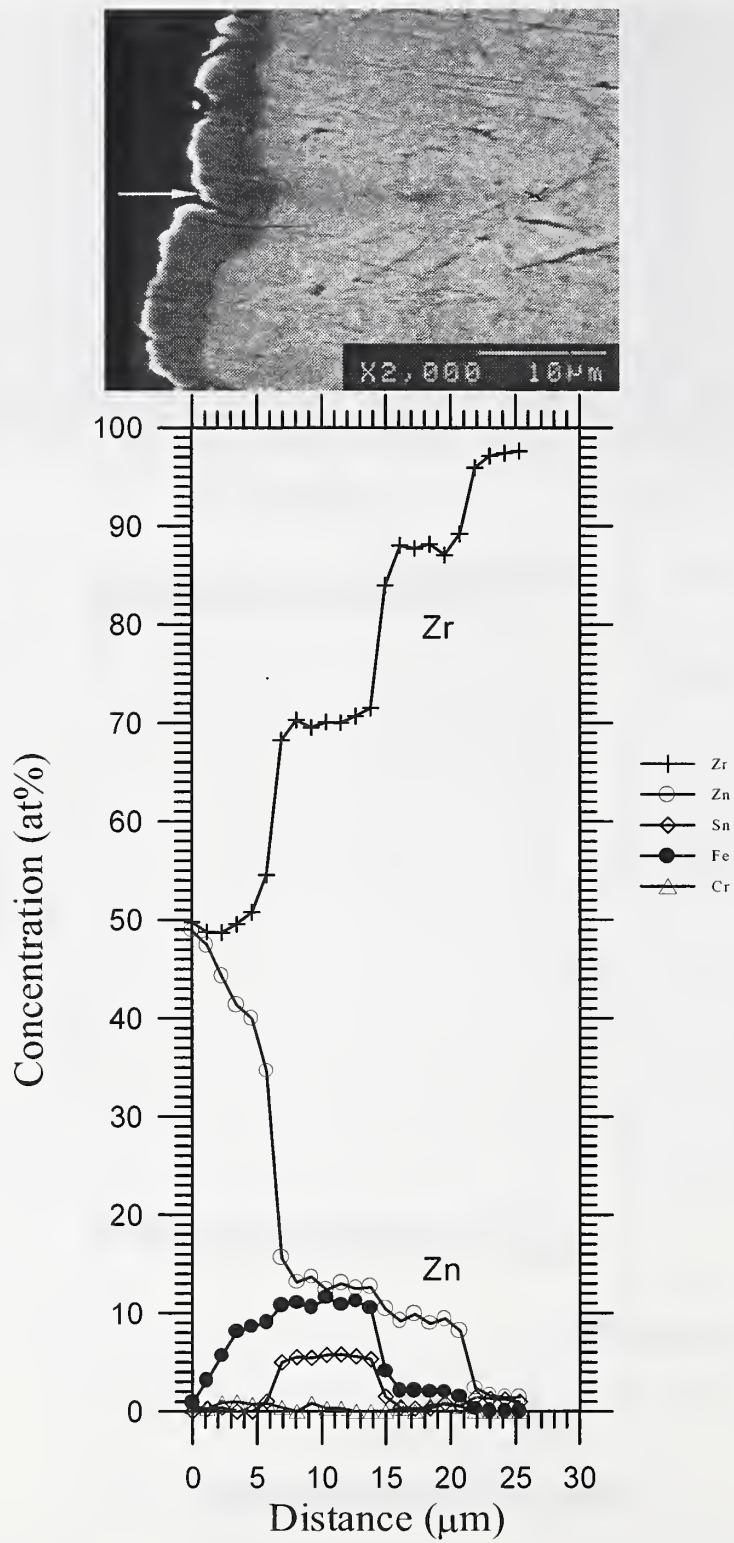
Figure A18. Zircaloy-4 TREX heat treated with zinc vapor at 725°C for 11.8 d, water quenched.

64
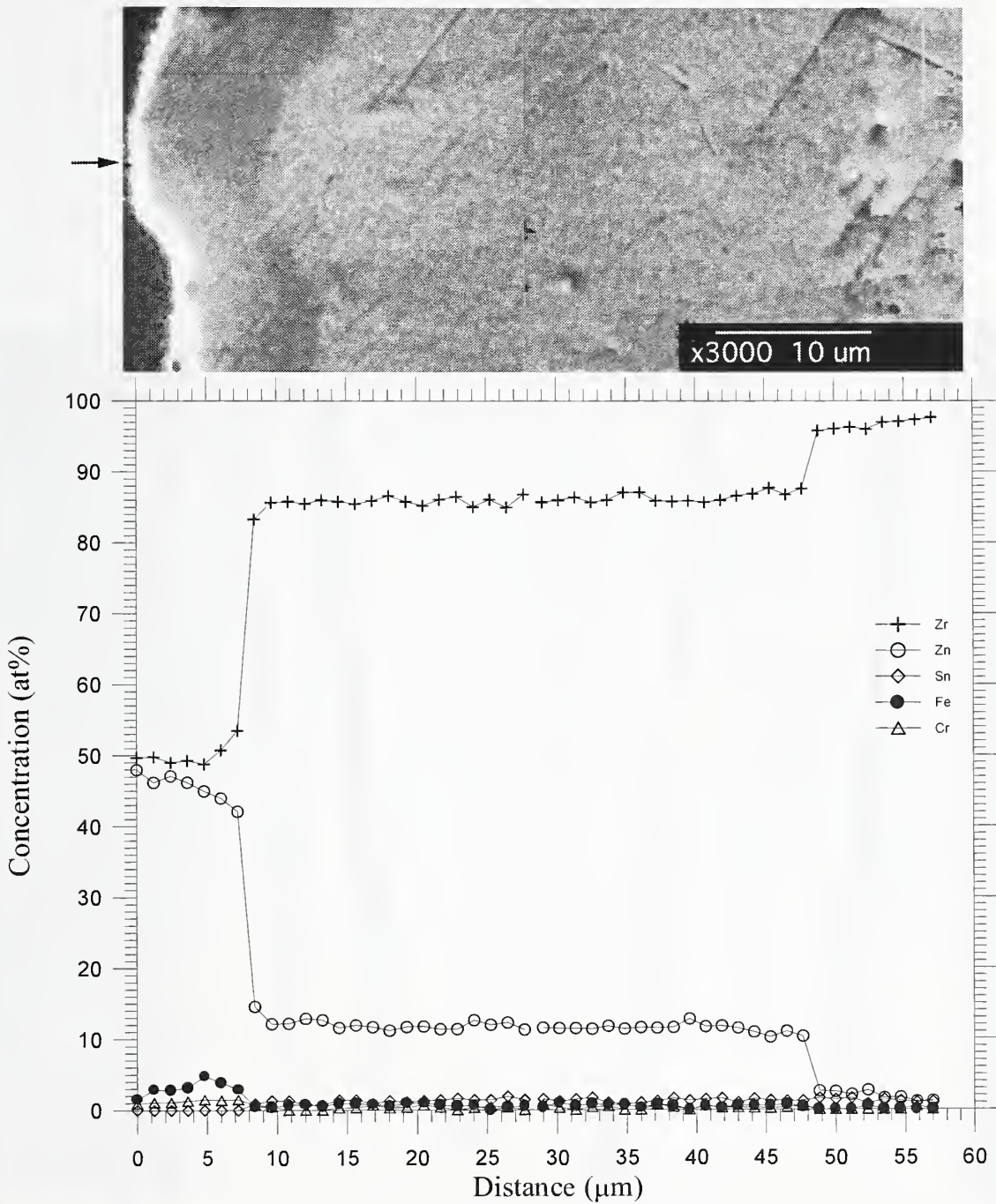
Figure A19. Zircaloy-4 tubing heat treated with zinc vapor at
725 °C for 39 d, water quenched.
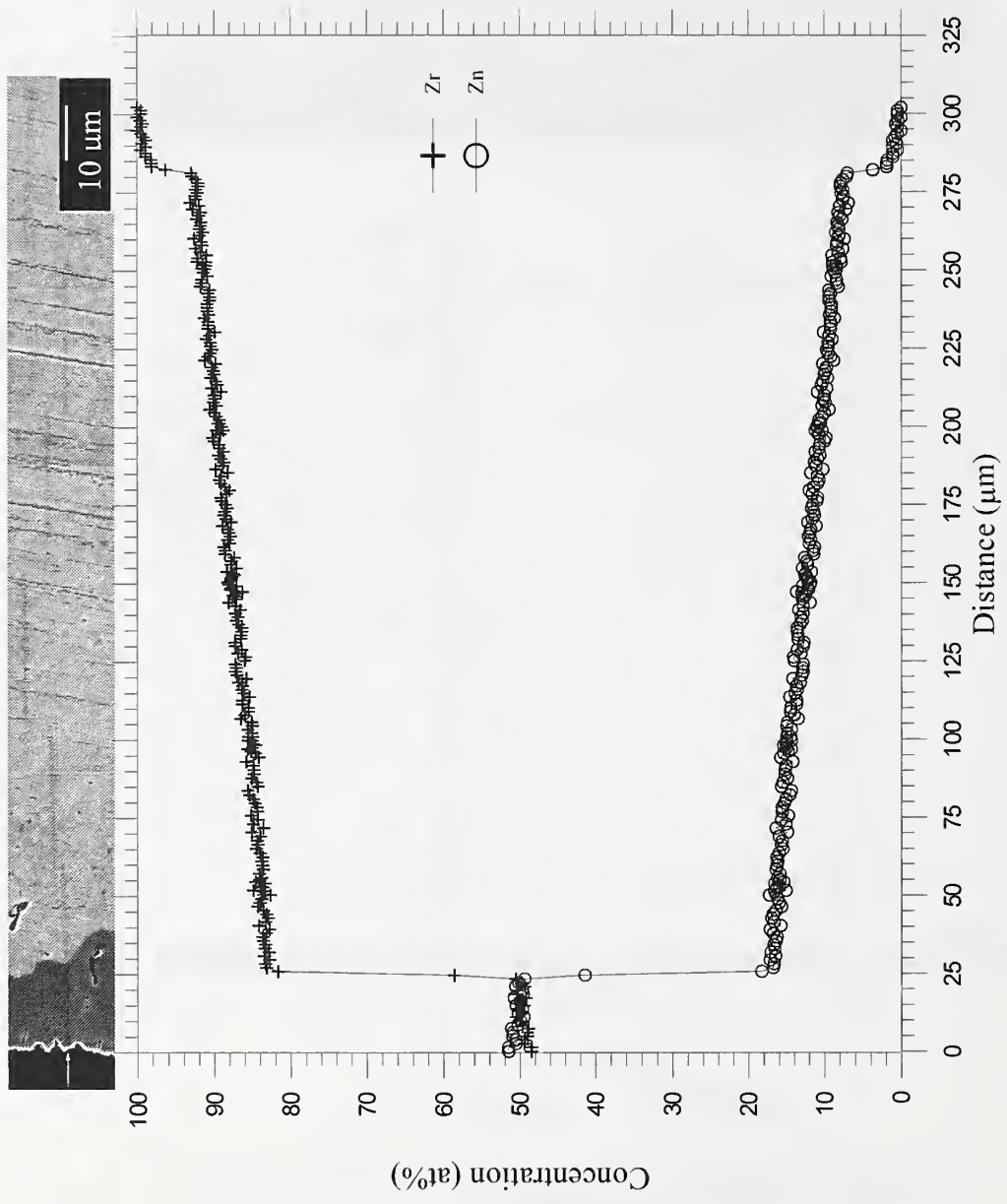
Figure A20. Nuclear grade zirconium heat treated with zinc vapor at 775 °C for 12 d, water quenched.
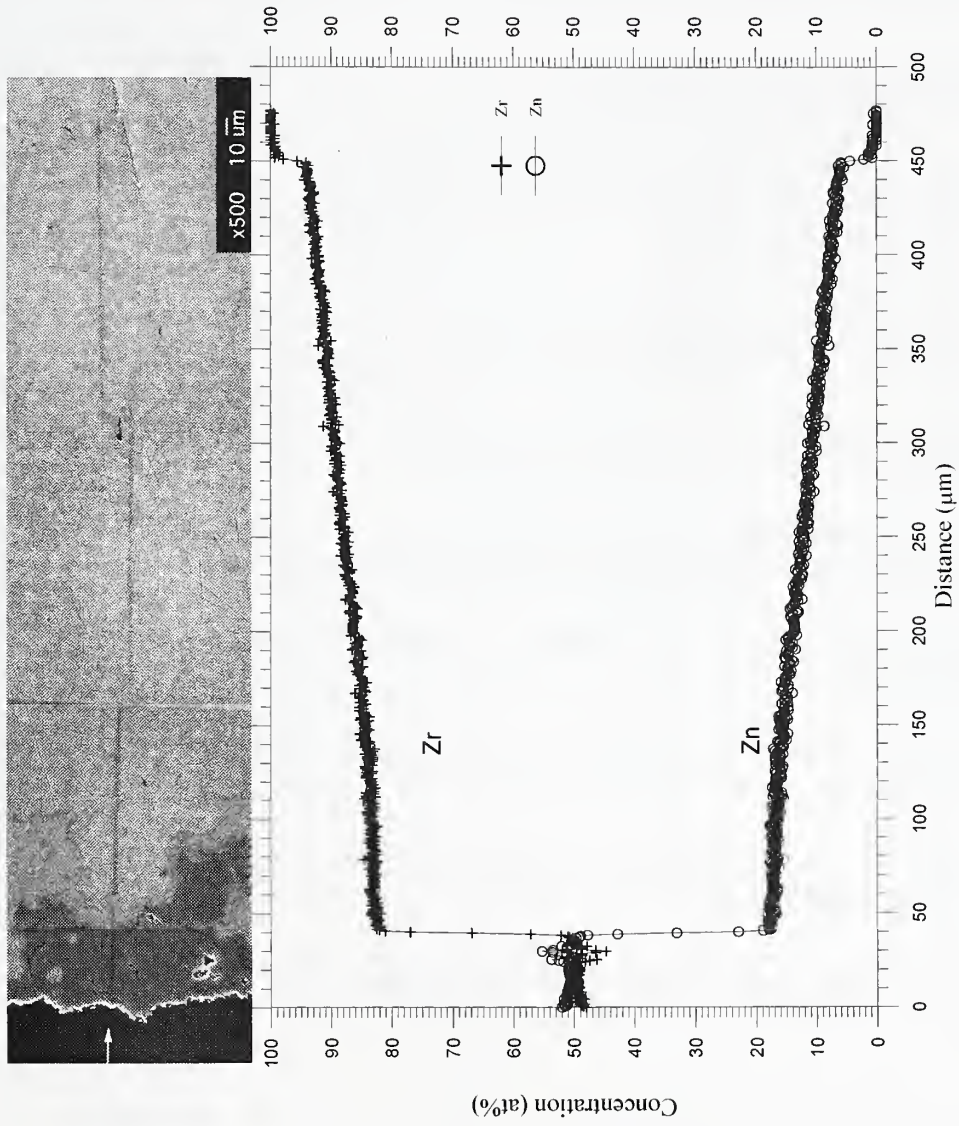
Figure A21. Nuclear grade zirconium heat treated with zinc vapor at 800 °C for 12 d, water quenched.

REFERENCES

1. *Viability Assessment of a repository at Yucca Mountain*, Yucca Mountain Project website http://www.ymp.gov/timeline/ops.htm, , 2/8/1999 , p4.

2. *NUREG-1536: Standard Review Plan for Dry Cask Storage Systems Section 4 - Thermal Evaluation*, Nuclear Regulatory Commission website http://www.nrc.gov/NRC/NUREGS/SR1536/part08.html, , 2/9/99, p 3,4.

3. *Onsite Storage of Spent Nuclear Fuel*, Nuclear Regulatory Commission website, http://www.nrc.gov/OPA/drycask/ , , 2/1999, p2.

4. Nonferrous Metal Products Section 2, ASTM Standard B350/B350M – 96, *Standard Specification for Zirconium and Zirconium Alloy Ingots for Nuclear Applications*, Annual Books of ASTM Standards, 1999

5. NRC bulletin 96-04, *Chemical, Galvanic, or other Reactions in Spent Fuel Storage and Transportation Casks*, July 1996, p 4.

6. *Binary Alloy Phase Diagrams*, ASM International, Materials Park, Ohio, Vol.3, 1990, p 3539,3541,3542.

7. Villars, P. and L.D. Calvert, Pearson's Crystallographic Data for Intermetallic Phases, ASM International, Materials Park, Ohio, vol. 3, 3rd ed., 1989, p3256

8. Rossteutscher, W. and K. Schubert, Z. Metallkd, *On Several T-Zn and T-Cd Alooy Systems*, 56, 1965, p730-734.

9. The Metallurgy of Zirconium, McGraw-Hill, edited by Lustman, Benjamin and Frank Kerze, Jr ,1955, p 5-14.

10. *Specific Metals and Alloys Section*, Metals Handbook, Ed. Lois A. Abel et al., vol. 2,10[th] ed., ASM International,1990, p667.

11. Thom, J.R.S., W.M. Walker, T.A. Fallon and G.F.S. Reising, *Boiling in Subcooled Water During Flow-up-Heated Tubes or Annuli*, Proc. Instn. Mech. Engrs.,180, Pt. C, 1965-66, p226-246.

12. Askeland, D.R., The Science and Engineering of Materials, PWS-Kent Publishing Co, 1984, p95,96,189.

13. Robert E. Reed-Hill and Reza Abbaschian, Physical Metallurgy Principles, PWS Publishing Co Boston, 3 ed , 1994 , p376-377.

14. F.J.J. van Loo, *Multiphase Diffusion in Binary and Ternary Solid-State Systems*, Great Britain, Prog. Solid St. Chem., Vol.20, 1990 ,pp. 47-99.

15. Porter, D.A., and K.E. Easterling, Phase Transformations in Metals and Alloys, London: Chapman and Hall, 2nd ed., 1995, p40.

16. Ursula Kattner thermodynamic assessment of zinc in α-brass based on M. Kowalski and P.J. Spencer. J Phase Equilibria, 14, 1993, p432-438.

17. Westinghouse Publication, *High Quality Zircaloy Tubing for Nuclear Applications*, 1984

18. Naylor, T.D. and J.H. Schemel, *Zircaloy Cladding Fabrication*, Sandvik Special Metals Corporation, American Nuclear Society, June 20, 1978 , p4.

19. Handbook of Chemistry and Physics, *Vapor Pressure Variation with Temperature*, CRC Press, 65th ed., 1985, p D-215.

20. Metals Test Methods and Analytical Procedures Section 3, ASTM Standard Test Method E112 - 96, *Standard Test Methods for Determining Average Grain Size*, Annual Books of ASTM Standards, 1999

21. VanderVoort, G.F., Metallography :Principles and Practice, Mc Graw –Hill, 1984 p701.